Relict basin closure and crustal shortening budgets during continental collision: An example from Caucasus sediment provenance

Eric Cowgill[1*], Adam M. Forte[1,2], Nathan Niemi[3], Boris Avdeev[3, 4], Alex Tye[3], Chad Trexler[1], Zurab Javakhishvili[5], Mikheil Elashvili[5], Tea Godoladze[5]

[1]University of California, Davis, CA, United States

[2]Now at Arizona State University, AZ, United States

[3]University of Michigan, MI, United States

[4]Deceased

[5]Ilia State University, Tbilisi, Georgia

*Corresponding author: Dr. Eric Cowgill, Earth & Planetary Sciences, One Shields Ave., University of California Davis, Davis, CA 95616; escowgill@ucdavis.edu; 530-754-6574.

Key Points:

1. U-Pb provenance indicates Greater Caucasus formed by post-collisional Cenozoic closure of a Mesozoic backarc likely ~350-400 km wide.
2. Post-collisional subduction/underthrusting of such relict basins helps account for shortening deficits and delayed plate deceleration.
3. Plate convergence should not be expected to balance upper-crustal shortening or the length of subducted slab following collision.

This is the author manuscript accepted for publication and has undergone full peer review but has not been through the copyediting, typesetting, pagination and proofreading process, which may lead to differences between this version and the Version of Record. Please cite this article as doi: 10.1002/2016TC004295

Abstract

Comparison of plate convergence with the timing and magnitude of upper-crustal shortening in collisional orogens indicates both shortening deficits (200-1700 km) and significant (10-40%) plate deceleration during collision, the cause(s) for which remain debated. The Greater Caucasus Mountains, which result from post-collisional Cenozoic closure of a relict Mesozoic back-arc basin on the northern margin of the Arabia-Eurasia collision zone, help reconcile these debates. Here we use U-Pb detrital zircon provenance data and the regional geology of the Caucasus to investigate the width of the now-consumed Mesozoic back-arc basin and its closure history. The provenance data record distinct southern and northern provenance domains that persisted until at least the Miocene. Maximum basin width was likely ~350-400 km. We propose that closure of the back-arc basin initiated at ~35 Ma, coincident with initial (soft) Arabia-Eurasia collision along the Bitlis-Zagros suture, eventually leading to ~5 Ma (hard) collision between the Lesser Caucasus arc and the Scythian platform to form the Greater Caucasus Mountains. Final basin closure triggered deceleration of plate convergence and tectonic reorganization throughout the collision. Post-collisional subduction of such small (10^2-10^3 km wide) relict ocean basins can account for both shortening deficits and delays in plate deceleration by accommodating convergence via subduction/underthrusting, although such shortening is easily missed if it occurs along structures hidden within flysch/slate belts. Relict-basin closure is likely typical in continental collisions in which

the colliding margins are either irregularly shaped or rimmed by extensive back-arc basins and fringing arcs, such as those in the modern South Pacific.

1. Introduction

Quantifying the deformational response of the continental lithosphere to plate collision is central for understanding fundamental earth systems such as geochemical cycling between the crust and oceans [*Li and West*, 2014; *Raymo and Ruddiman*, 1992; *Raymo et al.*, 1988], the impact of seaway closure on ocean circulation [*Allen and Armstrong*, 2008; *Haug and Tiedemann*, 1998], and environmental change in response to the growth of orogenic topography [*Ruddiman and Kutzbach*, 1989]. Active collisional orogens are particularly significant because they provide unique opportunities to relate the response of continents to the plate motions driving deformation [e.g. *Clark*, 2012]. However, crustal shortening measured in most active orogens is typically hundreds to thousands of kilometers less than post-collisional plate convergence [*Lippert et al.*, 2014; *McQuarrie et al.*, 2003; *van Hinsbergen et al.*, 2011; *Yakovlev and Clark*, 2014]. For example, in the India-Eurasia collision zone (Figure 1), total plate convergence (2400 to 3200 km) since the onset of collision at ~50 Ma exceeds the sum of known or inferred crustal shortening in Eurasia (1050 to 600 km) and India (675 ± 225 km) by at least 450 to 1700 km [*van Hinsbergen et al.*, 2011; *Yakovlev and Clark*, 2014], although lithospheric-scale balancing has been reported [e.g., *Guillot et al.*, 2003; *Replumaz et al.*,

2013; *Replumaz et al.*, 2014]. Likewise, the deficit of crustal shortening in the Arabia-Eurasia collision zone east of 48°E (Figure 1) is at least 220 to 420 km since 35 Ma, based on the difference between 750 to 950 km of post-35 Ma plate convergence and ~530 km of documented shortening (i.e., ~175 km in Eurasia, ~175 km in the Zagros, and ~180 km from Arabian underthrusting) [*McQuarrie and van Hinsbergen*, 2013] (Figure 1). It has proven challenging to identify the structural systems responsible for absorbing this missing shortening and thus reconcile such shortening deficits. Proposed solutions in both the India- and Arabia-Eurasia collisions include collisional ages younger than indicated by geologic observations [*Aitchison et al.*, 2007; *Ali and Aitchison*, 2006; *Boutlhol et al.*, 2013; *McQuarrie et al.*, 2003] or subduction of large portions of thinned continental or oceanic crust on the leading margin of the incoming continent [*Ballato et al.*, 2011; *McQuarrie and van Hinsbergen*, 2013; *Simmons et al.*, 2011; *van Hinsbergen et al.*, 2012]. Based on the Cenozoic evolution of the Greater Caucasus, here we describe a new mechanism for accommodating such shortening deficits, in which post-collisional subduction of a relict ocean basin accommodates convergence with minimal upper crustal shortening.

Active collisional orogens also provide unique opportunities to relate the response of plate dynamics to collision by determining how the balance of forces acting on the colliding plates change during collision to produce post-collisional deceleration of convergence [*Clark*, 2012; *Dewey et al.*, 1989; *Molnar and Lyon-Caen*, 1988; *Patriat and*

Achache, 1984]. For example, post-collisional deceleration of plate motion has been attributed to reduction in slab-pull following breakoff [*Capitanio and Replumaz*, 2013], increased buoyancy from continental subduction [*Capitanio et al.*, 2010], increased gravitational potential energy due to upper-plate thickening [*Austermann and Iaffaldano*, 2013; *Copley et al.*, 2010; *Flesch et al.*, 2001; *Molnar and Lyon-Caen*, 1988; *Molnar and Stock*, 2009], or viscous resistance to plate motion by the upper-plate mantle lithosphere [*Clark*, 2012].

The Arabia-Eurasia (Ab-Eu) collision is in the early stages of continental collision and provides an ideal location to investigate both shortening deficits and post-collisional deceleration of convergence. Relative to the India-Eurasia collision, the Ab-Eu collision has accumulated less total convergence because it is both younger (~35 vs. ~50 Ma) and slower (~20 vs. ~50 mm/yr) [e.g., *Hatzfeld and Molnar*, 2010]. In addition, the Ab-Eu collision appears to have a protracted early phase of soft collision that transitioned to a hard collisional mode at 20-17.5 Ma in Iran [*Ballato et al.*, 2011] to ~5 Ma in the Greater Caucasus (this study). Although the rate of convergence has slowed over time in both collisions [*Austermann and Iaffaldano*, 2013; *Clark*, 2012; *Copley et al.*, 2010; *Molnar and Stock*, 2009], it appears that the Ab-Eu relative motion did not significantly decelerate until ~5 Ma [*Austermann and Iaffaldano*, 2013], roughly 30 Myr after the onset of collision (Figure 1b) [e.g., *Allen and Armstrong*, 2008]. Specifically, rates of Ab-Eu convergence were 31 to 32 mm/yr both before and after the ~35 Ma onset of

collision [*McQuarrie et al.*, 2003]. While post-20 Ma rates are slower (~24 to 20 mm/yr), they are averaged over large time intervals (Figure 1b) and the ~20 mm/yr average rate since ~11 Ma appears to mask a more recent drop in rate from ~30 mm/y at ~5 Ma to ~19 mm/yr at present (Figure 1c) [*Austermann and Iaffaldano*, 2013].

A particularly striking aspect of the Ab-Eu collision zone is the existence of relict ocean basins that are now trapped within it, including the eastern Black Sea and the South Caspian Basin [e.g. *Zonenshain and Le Pichon*, 1986] (Figures 1a and 2). As used here, relict ocean basins include back-arc basins [*Karig*, 1971] such as the Japan Sea, remnant ocean basins [*Graham et al.*, 1975; *Ingersoll et al.*, 1995] such as the Bay of Bengal, or basins formed by transtensional rifting [*Taylor and Karner*, 1983], such as the Gulf of California, and include relict back-arc basins trapped within continental interiors, as suggested for the Junggar basin [*Carroll et al.*, 1990; *Hsü*, 1988]. When dormant, such basins are floored by ocean crust that is neither spreading nor subducting, [*Ingersoll*, 2012; *Ingersoll and Busby*, 1995]. "Relict ocean basin" is a general description that does not imply a particular basin-forming mechanism (e.g., back-arc rifting) or type of underlying crust (oceanic, continental, or transitional).

Both the eastern Black Sea and the South Caspian Basin are generally interpreted to be relict back-arc basins [e.g. *Brunet et al.*, 2003; *Knapp et al.*, 2004; *Okay et al.*, 1994; *Vincent et al.*, 2005; *Zonenshain and Le Pichon*, 1986]. The geology of the Greater Caucasus Mountains has long been understood to reflect Cenozoic closure and inversion

of the Greater Caucasus Basin, a Mesozoic marine back-arc basin similar to the Black Sea and South Caspian that originally formed during Jurassic back-arc rifting of the Lesser Caucasus volcanic arc from the southern margin of Eurasia during north-dipping subduction of Neotethys [*Adamia et al.*, 1977; *Adamia et al.*, 2011; *Gamkrelidze*, 1986; *Zonenshain and Le Pichon*, 1986]. However, the size of this basin and the role it has played in accommodating the Ab-Eu collision remain disputed.

Here we use U-Pb detrital zircon provenance data in combination with paleogeographic and paleotectonic reconstructions to determine if the basin was of sufficient size so that its closure could account for the discrepancy observed between plate convergence and crustal shortening. Our analyses indicate that early Jurassic to middle Miocene sandstones within the Greater and Lesser Caucasus were derived from one of two basic sources: a northern domain, characterized by grains older than ~230 Ma, and a southern domain, characterized by grains younger than ~170 Ma. This contrast in provenance reflects derivation from distinct sources on opposite sides of an intervening ocean basin that has since closed. These two sources are perhaps best exposed along the Girdiman Caj (River) in eastern Azerbaijan (approximately at location of sample SE-GC in Figure 2a), where two sections of Albian-Cenomanian strata are juxtaposed across the Zangi thrust [e.g., *Khain*, 2007]. To the north, the Cretaceous strata consist of deep-marine fine-grained carbonaceous sandstone and shale [*Kopp*, 1985], while to the south, the same age strata comprise andesitic lavas and associated coarse-grained volcaniclastic

rocks [*Abdulleyev and Samedova*, 1976]. The boundary separating these two packages of rocks represents the location of this former ocean basin, and thus a suture zone. However it is not defined by traditional geologic signs of a suture, e.g., obducted ophiolitic material or a melange zone, so it is best described as a cryptic or hidden suture [sensu, *Şengör*, 1984]. Integrating these new U-Pb detrital zircon analyses with prior work on regional geology, crustal structure, sediment provenance, and thermochronology suggests that subduction of a relict ocean basin during the early stages of continental collision can absorb significant convergence with minimal crustal shortening and deceleration of plate velocity.

2. Tectonic Setting

The Greater Caucasus defines the northern margin of the Ab-Eu collision zone between the Black and Caspian seas, and is located 400 to 700 km north of the topographic front on the northern margin of Arabia, with the range in values reflecting a westward increase in the width of this sector of the orogen (Figures 2a and 2b). From north to south, the main tectonic elements in the Caucasus region are the East European Craton and fringing Scythian Platform, the Greater Caucasus, the Rioni, Kartli, and Kura foreland basins, and the Lesser Caucasus Mountains (Figures 2a and 2b). The Lesser Caucasus were sutured with the Anatolide-Tauride-Armenian (ATA) block to the south, which is of Gondwanan affinity, along the Izmir-Ankara-Erzincan-Sevan-Akera (IAESA)

suture (Figure 2b) in Late Cretaceous [*Rolland et al.*, 2009; *Rolland et al.*, 2012] or Paleocene time [*Sosson et al.*, 2010]. In eastern Anatolia, south of the IAESA, the nature of the crust is disputed due to extensive Quaternary volcanic cover. One view is that it comprises a subduction-accretion complex (the East Anatolian Accretionary Complex or EAAC) of Upper Cretaceous and younger ophiolitic melange and Paleocene to Upper Oligocene flysch, with no continental basement [*Keskin*, 2003; *Şengör et al.*, 2003; *Şengör et al.*, 2008]. Another view is that it comprises the Anatolide-Tauride-Armenian continental block [*Oberhänsli et al.*, 2012; *Oberhänsli et al.*, 2010; *Rolland et al.*, 2012; *Sosson et al.*, 2010]. In both cases the southern margin of eastern Anatolia is bound by the Bitlis-Pötürge metamorphic massif, which is separated from Arabia to the south by the Bitlis-Zagros suture (Figure 2b). The Bitlis-Zagros suture is the main Neotethyan suture between Arabia and Eurasia [e.g., *Hempton*, 1985 and references therein; *Şengör et al.*, 2008] and is generally accepted to have closed in late Eocene to early Oligocene time [*Agard et al.*, 2005; *Allen and Armstrong*, 2008; *Ballato et al.*, 2011; *Boulton and Robertson*, 2007; *Hempton*, 1985; 1987; *Rolland et al.*, 2012; *Yilmaz*, 1993], although younger (i.e., late Miocene) ages have been proposed [*Ali et al.*, 2013; *Okay et al.*, 2010]. To provide structural and geologic context for our zircon provenance study, the following introduces the bedrock geology of the Caucasus region from north to south, followed by a summary of active tectonics.

2.1 East European Craton and Scythian Platform

The **East European Craton** (Baltica) comprises blocks of Archean continental crust (>2.54 Ga) enveloped within regions of Paleoproterozic (2.3-1.8 Ga) crust (Figures 1a and 2b) [e.g., *Bogdanova et al.*, 2008; *Wang et al.*, 2011]. The **Scythian Platform** fringes the southern margin of the East European Craton, although the nature and age of the Scythian basement are unclear due to extensive Mesozoic to Cenozoic sedimentary cover in the Indolo-Kuban and Terek basins and the intervening Stavropol high (Figure 2b) [*Natal'in and Şengör*, 2005; *Nikishin et al.*, 2011; *Nikishin et al.*, 2001]. This basement has been variably interpreted as a complex Paleozoic orogenic belt [*Belov et al.*, 1978; *Nikishin et al.*, 2011; *Nikishin et al.*, 2001] or a late Paleozoic island arc-forearc system subsequently duplexed by strike-slip faulting [*Natal'in and Şengör*, 2005]. It may also include Proterozoic crust of possible pan-African (i.e., Gondwanan) affinity [*Nikishin et al.*, 2011].

2.2 Greater Caucasus

The structural architecture and exposed geology of the Greater Caucasus orogen vary significantly along strike (Figure 2a) [*Ali-Zade et al.*, 2005; *Gudjabidze*, 2003; *Nalivkin*, 1976]. West of 44°E, the orogen is singly vergent and south-directed [*Forte et al.*, 2014]. From north to south this portion of the range comprises a north-dipping homocline of Lower Jurassic to Miocene (Sarmatian) strata unconformably overlying slivers of Cambrian and Devonian strata above a crystalline core of Variscan basement in

the hanging wall of the Main Caucasus Thrust; a complex system of north-dipping thrust sheets of Jurassic clastic and volcaniclastic strata; a south-dipping homocline of Jurassic to Sarmatian-aged strata at the southern mountain front; and a low-elevation foreland fold-thrust belt exposing Lower Cretaceous to upper Miocene (Pontian) strata [*Gudjabidze*, 2003; *Nalivkin*, 1976]. Between 44°E and 46°E, the range is doubly vergent but dominated by south-directed thrusts [*Forte et al.*, 2014]. From north to south, the main units here include a north-directed thrust belt exposing lower Miocene (Tarkhanian) to upper Miocene (Meotian/Pontian) strata on the northern margin of the range; north-directed thrust sheets of Jurassic to Cretaceous-aged strata [e.g., *Sobornov*, 1996]; a belt of Variscan crystalline basement; south-directed thrust sheets of Jurassic to Cretaceous clastic and carbonate strata lacking significant volcanic components; a zone of complex deformation involving Middle Jurassic to upper Miocene (Sarmatian) strata near the range front; and a foreland fold-thrust belt exposing upper Paleogene to upper Miocene (Pontian) strata [*Gudjabidze*, 2003; *Nalivkin*, 1976]. East of 46°E, the orogen is again singly vergent and south-directed [*Forte et al.*, 2014] but lacks exposed basement [*Ali-Zade et al.*, 2005; *Nalivkin*, 1976]. From north to south, main units here are Jurassic to Cretaceous clastic and carbonate deposits [*Kopp*, 1985] structurally juxtaposed across the north-dipping Zangi thrust [*Khain*, 2007] against similarly aged andesitic lavas and associated coarse-grained volcaniclastic rocks [*Abdulleyev and Samedova*, 1976] of the Vandam zone. The foreland fold-thrust belt exposes upper Miocene (Sarmatian) to

Pleistocene (Apsheronian) strata [*Forte et al.*, 2010; *Forte et al.*, 2013; *Forte et al.*, 2015; *Nalivkin*, 1976]. Within the Greater Caucasus, three domains are particularly significant for the present study (Variscan Basement, south-directed thrust belt, and the Vandam). .

The crystalline core of **Variscan Basement** is exposed west of ~45°E and comprises Late Paleozoic, arc-related granitic plutons, migmatite, and both ortho- and paragneiss [*Nalivkin*, 1973]. The northern margin of this domain is a suture with Scythia containing ecolgite-bearing blueschist with peak metamorphic conditions of 1.6 ± 0.2 GPa and 600 ± 40 °C, [*Perchuk and Philippot*, 1997] reached at 330 to 310 Ma, based on Sm-Nd and Lu-Hf garnet ages [*Philippot et al.*, 2001]. The southern edge of the basement domain is the Main Caucasus Thrust (Figure 2a) [e.g., *Somin*, 2011]. Early works describe the core of the Greater Caucasus as a mixture of Proterozoic through Paleozoic basement [*Belov et al.*, 1978; *Nalivkin*, 1973], but more recent geochronology (U-Pb zircon, Sm-Nd and Lu-Hf garnet, $^{40}Ar/^{39}Ar$ biotite and muscovite) suggests that most of the crystalline rocks are Late Paleozoic (Carboniferous-Permian) in age, with older Precambrian detrital zircons in some of the paragneiss [*Hanel et al.*, 1992; *Perchuk and Philippot*, 1997; *Philippot et al.*, 2001; *Somin*, 2011; *Somin et al.*, 2007; *Somin et al.*, 2006]. A preponderance of ~340-300 Ma granitic and metamorphic zircons in the core of the range suggest it is part of the broader Variscan-Hercynian orogenic belt that extends westward into Western Europe. The crystalline core is spatially associated with the Dizi metasedimentary series to the south of Devonian to Triassic age [*Adamia et al.*, 2011;

Somin, 2011], although contact relations between the Variscan basement and Dizi metasedimentary unit are unclear. The crystalline basement is locally intruded by mafic to intermediate composition dikes (Figure 3a) of reported Middle Jurassic age [*Gubkina and Ermakov*, 1989], and is depositionally overlain by upper Jurassic- and Cretaceous-aged shelf carbonates (Figure 2a) [e.g., *Nalivkin*, 1976].

South of the crystalline core is an active, south-directed **Thrust Belt** (i.e., the "Southern Slope Zone"), dominated by thrust sheets of middle-Jurassic to Pleistocene sedimentary rock originally deposited within both the Greater Caucasus Back-arc Basin and successor foreland basins that developed within the thrust belt [e.g., *Adamia et al.*, 2011; *Banks et al.*, 1997; *Dotduyev*, 1986; *Forte et al.*, 2014; *Forte et al.*, 2010; *Forte et al.*, 2013; *Philip et al.*, 1989]. The thrust belt was produced by Oligocene to Pliocene shortening [*Avdeev*, 2011; *Avdeev and Niemi*, 2011; *Forte et al.*, 2010; *Forte et al.*, 2013; *Sosson et al.*, 2010; *Vincent et al.*, 2007; *Vincent et al.*, 2011]. The northern part of the thrust belt comprises flysch deposits dominated by slate/shale and interbedded sandstone (Figure 3b) of Jurassic- to Cretaceous-age [*Kandelaki and Kakhazdze*, 1957]. Deeper (Early Jurassic) parts of this stratigraphic section are intruded by the same dikes of Middle Jurassic age [*Gubkina and Ermakov*, 1989] as in the crystalline basement of the MCT hanging wall (Figure 3a). Along the Inguri River in western Georgia (Figure 2a), the thrust belt contains a section of Early to Middle Jurassic-aged [*Gamkrelidze and Kakhazdze*, 1959] pillow basalts and overlying volcaniclastic breccia at least several

kilometers thick (Figure 3d). South of this volcanic series, the predominant rock type is Jurassic- and Cretaceous-aged [*Markus and Miroshanikov,* 2001] flysch and volcaniclastic breccia (Figure 3c), overlain by thick carbonates of Cretaceous age (Figure 2a) [*Dzhanelidze and Kandelaki*, 1957; *Gamkrelidze and Kakhazdze,* 1959]. Thrust sheets in the southernmost part of the thrust belt contain olistostromes within Paleogene-aged coarse clastic deposits that envelope carbonate blocks similar to the Cretaceous units to the north (Figure 3e) [*Banks et al.*, 1997; *Kandelaki and Kakhazdze,* 1957; *Vincent et al.*, 2007]. The southern edge of the thrust belt is defined by fault-propagation folds deforming upper Miocene to Plio-Pleistocene deposits in the Rioni, Kartli, and Kura basins (Figure 2a) [e.g., *Forte et al.*, 2010; *Forte et al.*, 2013].

The **Vandam zone** is a narrow belt of primarily volcaniclastic rocks exposed in south-directed thrust sheets along the southeastern margin of the Greater Caucasus in Azerbaijan (around sample SE-GC on Figure 2a) [*Abdulleyev and Samedova,* 1976; *Safarov*, 2006]. These rocks have previously been described as Jurassic to Cretaceous in age [*Khain and Shardanov,* 1960] and are primarily mafic to intermediate in composition [*Safarov*, 2006]. Compositionally, they are very similar to Jurassic and Cretaceous aged volcanic rocks encountered at the base of deep wells within the Kura Basin [e.g., *Agabekov and Moshashvili,* 1978; *Shikalibeily et al.*, 1988] and within the Lesser Caucasus Arc (Figure 2a) [e.g., *Kopp and Shcherba*, 1985].

2.3 Lesser Caucasus

South of the Greater Caucasus and its flanking foreland basins, the northern margin of the Lesser Caucasus Mountains is defined in the west and east by north-directed Cenozoic thrust systems in the Achara-Trialet and Talysh, respectively (Figure 2a) [e.g., *Allen et al.*, 2003; *Banks et al.*, 1997; *Vincent et al.*, 2005]. Less clear is the extent to which such north-directed thrusting characterizes the intervening northern margin of the Lesser Caucasus (Figure 2a). Three subdomains of the Lesser Caucasus are noteworthy in terms of provenance: the Dzirula-Khrami-Loki Massifs, the Achara-Trialet and Talysh Belts, and the Lesser Caucasus Arc (Figure 2a).

The **Dzirula-Khrami-Loki Massifs** are fragments of Variscan and older basement very similar to the crystalline core of the Greater Caucasus (Figure 2a) [*Gamkrelidze and Shengelia*, 2001; *Gamkrelidze et al.*, 1981; *Mayringer et al.*, 2011; *Rolland et al.*, 2016; *Zakariadze et al.*, 2007]. In general, they expose Proterozoic to Carboniferous-aged metamorphic and igneous rocks that are both intruded and overlain by Mesozoic to early Cenozoic volcanic and volcaniclastic units [*Gamkrelidze and Shengelia*, 2001; *Zakariadze et al.*, 2007]. The basement includes MORB-type metabasic rocks (804 ± 100 Ma from whole-rock Sm-Nd) intruded by mafic/intermediate plutons (~750-540 Ma from U-Pb zircon, Rb-Sr whole rock and Sm-Nd mineral isochron) inferred to be an island arc complex built upon oceanic crust and then accreted to the Nubian shield of Gondwana [*Zakariadze et al.*, 2007]. These peri-Gondwanan fragments

are generally thought to have rifted from Gondwana via back-arc rifting above a south-dipping subduction zone in the early Paleozoic. They were accreted to the southern margin of Eurasia by ~350 Ma via closure of proto-Tethys, and were then subjected to high pressure-low temperature metamorphism from 329-337 Ma [*Rolland et al.*, 2011] and widespread granitic intrusion along the active Eurasian continental margin from 330-280 Ma above a north-dipping subduction zone along the northern margin of Paleotethys [e.g., *Rolland et al.*, 2016; *Zakariadze et al.*, 2007]. However, *Rolland et al.* [2016] question the robustness of the Rb-Sr and Sm-Nd dates due to the extensive Variscan metamorphic overprint and protracted residence of the samples in the upper plate of a long-lived Mesozoic subduction zone. In the Dzirula Massif, mafic to intermediate intrusive rocks record a crystallization age of ~540 Ma (upper intercept of U-Pb zircon discordia chord) with a metamorphic overprint at 338 ± 5 Ma (concordant U-Pb zircon rims), along with Variscan zircon crystallization ages of 335 to 320 Ma [*Mayringer et al.*, 2011; *Rolland et al.*, 2016]. In the Khrami Massif, zircons from a granodiorite reworked to migmatite yielded core ages of 474 ± 3 Ma and Variscan rims ages of 343 ± 2 Ma [*Rolland et al.*, 2016].

The **Achara-Trialet and Talysh Belts** are located along the northwestern flank of the Lesser Caucasus Mountains in Georgia and in the Talysh Mountains of Azerbaijan, respectively (Figure 2a), and predominantly comprise late Mesozoic to Cenozoic volcanic and volcaniclastic rocks [*Azizbekov and Dzotsenidze,* 1971]. Both regions

appear to have been narrow extensional basins that opened during the Cretaceous-Eocene and were filled with a mixture of sedimentary and volcanic deposits [*Adamia et al.*, 1974; *Kazmin et al.*, 1986; *Yilmaz et al.*, 2000]. In the Achara-Trialet belt, Cretaceous and Lower Eocene aged carbonate and flysch, locally intruded by dikes, are overlain by thick successions of Eocene to Oligocene aged volcanic and volcaniclastic rocks that are variably interpreted as indicative of arc or post-collisional volcanism [*Yilmaz et al.*, 2000]. These rocks are deformed by a series of north-vergent thrusts and folds (Banks et al., 1997; Robinson et al., 1997). In the Talysh, ~10 km of middle Eocene sedimentary and mafic volcanic rocks [*Kazmin et al.*, 1986] are interpreted to reflect back-arc rifting north of the Neo-Tethyan subduction zone [*Vincent et al.*, 2005].

The **Lesser Caucasus Arc** comprises a portion of the Lesser Caucasus Mountains north of the IAESA suture (Figure 2a). This belt is a remnant of a large volcanic arc or arc system that was active from Late Jurassic to Cretaceous time, with punctuated thermal events at 183, 166, and 114 Ma [*Rolland et al.*, 2011], and is thought to be continuous with the Pontide arc in Eastern Turkey [*Yilmaz et al.*, 2000]. Volcanism resulted from north-directed subduction along the southern flank of the Lesser Caucasus, roughly in the location of the IAESA suture (Figure 2b) [*Adamia et al.*, 1977; *Gamkrelidze*, 1986; *Kazmin et al.*, 1986; *Zonenshain and Le Pichon*, 1986]. The Greater Caucasus basin opened as a back arc of the Lesser Caucasus Arc, to the north in present coordinates. Geochronologic and geochemical data from Jurassic to Eocene igneous

rocks of the Lesser Caucasus indicate a subduction source [*Mederer et al.*, 2013; *Moritz et al.*, 2016; *Sahakyan et al.*, 2016]. The modern structural architecture of active faults in the Lesser Caucasus is poorly understood, with north-directed thrusting, south-directed thrusting, and strike-slip faults all proposed as dominant structures [*Koçyiğit et al.*, 2001; *Philip et al.*, 1989; *Rebaï et al.*, 1993]. More recent work argues for a strike-slip regime [*Avagyan et al.*, 2010].

2.4 Active Tectonics & Cenozoic Shortening

Between the Black and Caspian seas, 50 to 70% of present-day, orogen-perpendicular Ab-Eu convergence is localized in the Caucasus [e.g., *Jackson*, 1992; *McClusky et al.*, 2000; *Reilinger et al.*, 2006]. Prior workers hypothesized that much of this shortening was localized on thrust systems at the southern topographic front of the Greater Caucasus, such as the Main Caucasus Thrust in Azerbaijan [*Allen et al.*, 2004; *Philip et al.*, 1989; *Reilinger et al.*, 2006]. However, new work shows that east of 45ºE, most active shortening is accommodated to the south of the topographic front, within the Kura fold-thrust belt [*Forte et al.*, 2014; *Forte et al.*, 2010], with southward propagation of the deformation front occurring at ~2-1.5 Ma [*Forte et al.*, 2013]. East of 45°E, the Greater Caucasus Mountains overlie a north-dipping zone of subcrustal seismicity interpreted as a subducting slab of Kura basin basement [*Khain and Lobkovskiy*, 1994; *Khalilov et al.*, 1987; *Mellors et al.*, 2012; *Mumladze et al.*, 2015; *Skolbeltsyn et al.*, 2014]. The down-dip extent of seismicity implies a slab length of 130 – 280 km

[*Mumladze et al.*, 2015], as explained in the supplement. The lack of such deep seismicity west of 45°E is inferred to result from recent slab breakoff beneath the western part of the Greater Caucasus [*Mumladze et al.*, 2015].

Estimates of total shortening across the Caucasus span an order of magnitude. Paleomagnetic data imply values as high as ~900 ± 350 km for shortening across the combined Greater and Lesser Caucasus [*Bazhenov and Burtman*, 1989], with recent work indicating that the South Armenian block (Figure 2b) was no more than 1000 km from the southern margin of Eurasia in the Late Cretaceous [*Meijers et al.*, 2015]. *Ershov et al.* [2003] estimated 300 km of shortening based on crustal-scale area balancing of the orogen and an assumption of an original crustal thickness of 15-17 km. Estimates of ~200 km of shortening in the Greater Caucasus are based on reconstruction of folding, estimated fault offsets, and original patterns of sedimentary facies [*Dotduyev*, 1986]. At ~42°E in western Georgia, we obtain a minimum shortening estimate of 130 km, based on line-length balancing of a crustal-scale cross section (Figure 4) that we constructed from the surface geology reported on 1:200,000-scale Soviet geologic maps. However, ongoing geologic mapping in the vicinity of the surface trace of this cross section indicates that this estimate is too low; future refinement of this shortening estimate is expected [e.g., *Trexler et al.*, 2015]. The smallest shortening estimate (~25 km) is implied by comparison of the present width of the range to a presumed original basin width of ~80 km in the middle Eocene, prior to closure [*Nikishin et al.*, 2011].

3. Methods

Detrital zircon geochronology is a well-established technique for determining sediment provenance patterns and defining tectonostratigraphic correlations [*Andersen*, 2005; *Catalán et al.*, 2004; *Dickinson and Gehrels*, 2003; *Fedo et al.*, 2003; *Gehrels*, 2012; *Gehrels and Dickinson*, 1995; *Kelty et al.*, 2008; *Weislogel*, 2008; *Weislogel et al.*, 2006]. In this method, U-Pb isotopic analyses of multiple (>100), randomly selected individual zircon grains are used to determine the distribution of single-grain ages within a sample. The frequency of these single-grain ages are commonly interpreted as reflecting the areal distribution of the ages of rocks exposed in the sediment source area at the time of deposition [e.g., *Gehrels and Dickinson*, 1995], and samples with dissimilar age groups are interpreted to have been sourced from distinct source areas [e.g. *Andersen*, 2005; *Gehrels*, 2012].

3.1 Sampling Strategy

The size and geometry of the Greater Caucasus basin are poorly constrained [e.g., *Adamia et al.*, 2011; *Golonka*, 2007; *Nikishin et al.*, 2011]. To determine if the basin was of sufficient size so that its closure could account for discrepancies between plate motions and crustal shortening, we conducted U-Pb analyses of detrital zircons from 8 samples to characterize the sources of the homogenous flyschoid sediments of the Greater Caucasus Basin and sediments derived from arc volcanics within the Lesser Caucasus (Figure 2a; Table S1). We focus on characterizing samples on opposite sides of the south-

directed thrust belt in the Greater Caucasus, because this belt is inferred to result from inversion of the Greater Caucasus relict back-arc basin and is located between Scythia and the East European Craton to the north and the Lesser Caucasus to the south. Thus, we infer it may contain a cryptic or hidden suture zone [e.g., *Şengör*, 1984]. In detail, the goal was to determine if the Greater Caucasus Basin was large enough to prevent sedimentary exchange across it prior to Cenozoic closure. The samples comprise two pairs of sandstone samples largely spanning the thrust belt in the Greater Caucasus and four modern sediment samples from rivers draining the south flank of the Greater Caucasus (Inguri and Kumuk), the Lesser Caucasus (Tovuz), and the Achara-Trialet (Kura upper catchment). We combine these results with the limited detrital zircon data available for the Caucasus region (Table S1), including all reported analyses of Mesozoic [1 sample, *Allen et al.*, 2006] and Oligo-Miocene-aged sandstones [5 samples, *Vincent et al.*, 2013] (Figures 2a and 2b), as well as modern sediment from large modern rivers draining into the Caucasus region from the Eurasian continent (Don, Dnieper, and Volga Rivers in Russia) [*Wang et al.*, 2011] (Figure 1a). We report depositional ages for previously published Cenozoic samples using both the Paratethyan and international chronostratigraphic stages (e.g., Chokrakian; Langhian) as originally reported [*Vincent et al.*, 2014; *Vincent et al.*, 2013]. We exclude earlier detrital zircon studies of the modern Volga [*Allen et al.*, 2006; *Safonova et al.*, 2010] and Don [*Safonova et al.*, 2010], because they conform with the results of *Wang et al.* [2011]. Likewise, we do not include detrital

zircon analyses from 4 samples of the Lower Pliocene Productive Series on the Apsheron Peninsula [*Allen et al.*, 2006] due to their small sample sizes (~60 grains), young depositional ages, and restricted stratigraphic and geographic range.

3.2 Analytical Techniques

In the present study, we performed U-Pb isotopic analyses of zircons from 8 samples (Figure 2a) using laser ablation multi-collector inductively coupled plasma mass spectrometry (LA-MC-ICPMS) at the Arizona LaserChron Center following analytical procedures summarized in the supplement and described by *Gehrels et al.* [2006] and *Gehrels et al.* [2008]. We visualized the detrital age distributions (Figure 5) using both kernel density estimation (KDE) and probability density plots (PDP) generated with the DensityPlotter software [*Vermeesch*, 2012], which employs algorithms for adaptive bandwidth selection [*Botev et al.*, 2010] and log-transformation to visualize both young and old fractions [*Brandon*, 1996]. We compared age populations between samples both subjectively, using visual comparison of the PDP and KDE curves, as suggested by *Pullen et al.* [2014] (Figure 5a), and quantitatively, using the likeness metric for comparing PDPs (Figure 5c and 5d) [*Satkoski et al.*, 2013]. Additional information on analytical details, explanations of both PDP and KDE plots, selection of quantitative comparison metrics, and locations of additional provenance analyses previously reported by *Vincent et al.* [2013] are supplied in the Supplementary Information.

4. Results

Ages from this study are reported in Table S2 and shown as KDE and PDP curves on Figure 5a, on concordia diagrams in Figure S2, and as cumulative density functions in Figure S3. Likeness values are shown on Figure 5d and reported in Table S3.

4.1 Sandstone

Sandstone samples NE-GC and NW-GC, in the northern part of the thrust belt, are characterized by broad distributions of Mesozoic and Paleozoic ages (Figures 2a and 5a). In the west, sample NW-GC has a Lower Jurassic depositional age [*Gamkrelidze and Kakhazdze*, 1959] and is dominated by 300-800 Ma zircons, while to the east, Tithonian [*Khain and Shardanov*, 1960] sample NE-GC mainly contains 150-530 Ma zircons, with a tail extending past 2.0 Ga (Figure 5a and Table S2). In sharp contrast, sandstone samples SW-GC and SE-GC from the southern part of the thrust belt lack statistically significant populations (i.e., > 3) of early Mesozoic and Paleozoic-aged grains (Figures 2a and 5a). Instead, they yield age distributions dominated by single narrow peaks of Jurassic to Cretaceous age; i.e., ~170 Ma for sample SW-GC in the west and ~100 Ma for sample SE-GC in the east, which has a Cenomanian depositional age [*Khain and Shardanov*, 1960]. A statistically significant peak at ~27 Ma in sample SW-GC (5 analyses from 3 grains) indicates an Oligocene maximum depositional age that is much younger than its previously mapped Bajocian (Jurassic) age [*Gamkrelidze and Kakhazdze*, 1959].

4.2 Modern River Sediment

Modern sediments in the Inguri and Kumuk rivers draining the fold-thrust belt on the southern margin of the Greater Caucasus have age spectra dominated by 170-800 Ma zircons, with no younger peaks (Figures 2a and 5a). In contrast, younger peaks dominate in modern sediments from the Tovuz River, which drains the Lesser Caucasus, and the upper catchment of the Kura River, which drains the Achara-Trialet belt (Figures 2a and 5a). The Tovuz sample is dominated by 80-170 Ma grains, with no statistically significant older peaks. The Kura River contains peaks at 6-10 Ma and 40-50 Ma, with a spread of ages between 80 and 250 Ma (Figure 5a), also with no statistically significant older peaks.

5. Discussion

5.1 Provenance Domains

Previous detrital zircon characterization of potential sediment source areas is largely lacking in the Caucasus region. To address this problem, we analyze our results together with those from other workers using the Likeness-value technique for comparing zircon age spectra [*Satkoski et al.*, 2013] (Figure 5). The likeness value (L) is the absolute value of the difference between 2 zircon age spectra probability density functions [*Satkoski et al.*, 2013], where L = 1 represents identical samples, L = 0.5 represents samples with an equal number of age peaks that overlap as don't overlap, and L = 0

represents samples with no overlapping age peaks. However, L is also a function of sample size. Using a recently published 4000-grain zircon U-Pb age sample set [*Pullen et al.*, 2014], we find that the average L value for a 100-grain sample (typical of the data from the Caucasus) is 0.77 (Figure 5c). Therefore, we normalize the L values for pair-wise comparisons of the Caucasus detrital data by this value, and visualize the result using a correlation matrix (Figure 5d), where blue (yellow) colors represent small (large) values of normalized L and thus low (high) degrees of similarity.

This comparison, which is one of many possible quantitative comparisons [e.g., *Gehrels*, 2014], suggests four principal age spectra components. An **East European Craton (EEC) component** (Figure 5d) is comprised of predominantly Proterozoic and Archean grains, with subordinate Paleozoic grains, and is seen in modern rivers that drain the Eurasian craton (Dnieper, Don, Volga), and Oligo-Pliocene sedimentary rocks found north of the Greater Caucasus (ILN#13_700, WC139/1) (Figure 1). A **Variscan component** (Figure 5d) is seen in samples from the Greater Caucasus range (NE-GC, NW-GC, GC41), and in modern rivers that drain that range (Inguri, Kumuk), as well as in Oligocene-aged sedimentary rocks apparently derived from Variscan basement blocks in the Lesser Caucasus (e.g. Dzirula) that were rifted off of the south Eurasian margin (WG95/1) [*Vincent et al.*, 2013]. This component chiefly comprises Paleozoic grains, with a few older grains, and a peak of Jurassic (~170 Ma) ages. A **Mixed component** (Figure 5d) shows affinity to both the EEC and Variscan components, and is found in

Oligo-Miocene strata in the western Greater Caucasus (WG66c/2, WC99/3) [*Vincent et al.*, 2013]. A **Lesser Caucasus component** is found in the southwestern Greater Caucasus (SW-GC) and in one modern river (Tovuz) that drains the Lesser Caucasus (Figure 5d). It consists almost exclusively of Mesozoic grains, although minor components of both older and younger grains are present. Two additional samples show no strong affinities to other samples: A sample from the southeastern Greater Caucasus (SE-GC), in the Vandam zone of Lesser Caucasian affinity, shows a nearly unimodal age peak in the mid-Cretaceous. This sample is a proximal volcaniclastic sequence, and likely preserves grains from a single eruptive sequence. A sample from the Kura River has weak affinity to samples of all other groups, and likely is composed of a mixture of all four other domains (Figure 5d).

Comparing the spatial and temporal distributions of the samples within these components yields several key observations. (1) The Variscan basement and associated rocks that comprise the Greater Caucasus are distinct (in terms of zircon age spectra) from zircons derived from the East European Craton. (2) Modern rivers draining the thrust belt on the south flank of the Greater Caucasus have almost no zircons of affinity with the East European Craton. (3) At least some Cenozoic sedimentary rocks south of the Greater Caucasus contain grains of affinity with the East European Craton (e.g., WG99/3 (Oligocene) and WG66c/2 (Middle Miocene)), suggesting growth of the Greater Caucasus Mountains has only recently defeated south-flowing rivers crossing the East

European Craton and Variscan domains. (4) A Jurassic (~170 Ma) age peak is present in both the Variscan component and the Lesser Caucasus component; however, the Variscan component does not contain younger Mesozoic age peaks that otherwise characterize Lesser Caucasus-affinity rocks or modern rivers that drain the Lesser Caucasus, such as the Tovuz and Kura).

5.2 Paleogeography of Northern and Southern Provenance Domains

Three variables must be tracked for each sample when evaluating the paleogeographic implications of the detrital zircon results and additional provenance data discussed below: the depositional age, the provenance domain, and the geographic location relative to the Greater Caucasus thrust belt. Comparison of sample locations (Figure 2a) with provenance associations (Figure 5) indicates that samples from the northern part of the Caucasus region generally show Variscan provenance, whereas those from the southern part of the Caucasus region show affinity with the Lesser Caucasus Arc. The northern (Variscan) and southern (Lesser Caucasus) provenance domains are separated by the thrust belt along the southern flank of the Greater Caucasus (Figure 6).

The northern (Variscan) domain is defined by the broad distribution of early Mesozoic to Neoproterozoic ages (230 to 800 Ma) seen in (a) Jurassic sandstone samples NE-GC and NW-GC from this study and GC41 from *Allen et al.* [2006], (b) an early Oligocene (Maykopian; middle Rupelian) sample in the northern part of the thrust belt near Sochi (WC99/3), a middle Miocene (Chokrakian; Langhian) sample from the middle

of the thrust belt in the southwestern Greater Caucasus (WG66c/2), an Oligo-Miocene (middle Maykopian; Chattian-Aquitanian) sample from the Indolo-Kuban basin north of the range (ILN#13_700), and Mio-Pliocene (Kimmerian; late Messinian-Zanclean) sample from the Taman peninsula (WC139/1) to the north and west of the thrust belt [*Vincent et al.*, 2013] (Figures 1, 5, and 6). This domain also contributes modern sediment to the Inguri and Kumuk rivers (Figures 5 and 6). These ages indicate that Mesozoic sedimentary deposits in the northern part of the Greater Caucasus thrust belt were derived from Paleozoic to early Mesozoic sources dominated by Variscan basement exposed along the northern margin of the Greater Caucasus Basin. The low abundances of Precambrian grains in both the Mesozoic samples and modern Inguri and Kumuk River sediments suggests the EEC was not an important sediment source during Mesozoic opening and Cenozoic closure of the Greater Caucasus Basin [e.g., *Vincent et al.*, 2013]. However, the presence of peri-Gondwanan ages in some of the samples is consistent with zircon U-Pb crystallization ages throughout Iran in the Lut, Central, and Sanandaj-Sirjan zones [*Hassanzadeh et al.*, 2008]. These ages appear in sample NW-GC, and are a minor component of the Inguri sample, but are otherwise mostly absent. Thus, while there may have been a piece of Cimmeria in the region during the Jurassic as a source for sediments now in the western Greater Caucasus, it no longer appears to be a significant sediment source. The northern source defined the northern margin of the relict ocean basin from Middle Jurassic to Eocene(?) time, and is now exposed within the core

of the Greater Caucasus (Figures 2a, 5 and 6). Importantly, the lack of grains younger than ~170 Ma in modern sediments of the Inguri and Kumuk rivers attests to the lack of a young age component in this northern domain.

In contrast, the southern (Lesser Caucasus) domain is characterized by ages ~170 Ma (Middle Jurassic) and younger, and almost entirely lacks the old ages that define the northern domain (Figures 5 and 6). Samples of south-domain affinity include (a) Mesozoic sandstone sample SE-GC at the southern edge of the thrust belt in the southeastern Greater Caucasus, (b) Cenozoic (post-27 Ma) sandstone sample SW-GC, in the southwestern part of the thrust belt, and (c) modern sediments in rivers draining the Lesser Caucasus (i.e., Tovuz and Kura). In these samples, the almost complete lack of older grains derived from the northern source indicates that Mesozoic and Cenozoic sediments in the southern domain were sourced almost exclusively from a Jurassic-to-Eocene-aged island arc complex along the southern edge of the basin. The analysis of likeness values in Figure 5d indicates minimal evidence for mixing between the northern (Variscan) and southern (Lesser Caucasus) domains, in contrast to evidence for mixing of EEC and Variscan domains in two samples from the westernmost Greater Caucasus.

5.3 Location of Hypothesized Suture in the Greater Caucasus

The generally distinct age distributions between samples with Variscan provenance affinity in the northern Greater Caucasus and those with Lesser Caucasus affinity to the south suggests the presence of a significant crustal boundary along the

southern flank of the Greater Caucasus, which we interpret as a cryptic suture zone within the Greater Caucasus thrust belt. This inferred suture zone is shown schematically in Figure 6, although the geometry is approximate because it is simplified and important aspects remain to be established. Specifically, more work on the internal structure of the thrust belt is needed to determine if the location and geometry of the suture can be refined into a discrete structure or set of structures. Details of the basin evolution remain uncertain because samples for detrital zircon and other provenance studies are generally from deposits now exposed in south-directed thrust sheets produced by Miocene to Pliocene deformation [*Avdeev*, 2011; *Avdeev and Niemi*, 2011; *Forte et al.*, 2010; *Forte et al.*, 2013; *Sosson et al.*, 2010; *Vincent et al.*, 2011] that remains to be palinspastically restored. As a result, the original positions of the samples within the basin at the time of deposition remain largely unknown.

As shown on the schematic cross sections in Figure 6 and explained below, we infer that the Greater Caucasus basin was wide during latest Cretaceous to Paleocene time, but narrow both during middle Jurassic opening and late Miocene closure of the back arc basin. The lack of significant overlap in ages between the northern (Variscan) and southern (Lesser Caucasus) domains indicates a lack of sedimentary exchange across the Greater Caucasus Basin from the late Mesozoic until at least Oligocene time.

The southern domain also contains Variscan basement in the Dzirula, Khrami and Loki Massifs (Figures 2a and 6) [*Nalivkin*, 1976; *Robinson et al.*, 1997; *Sosson et al.*,

2010; *Zakariadze et al.*, 2007]. These massifs were rifted from the Variscan orogenic belt along the southern margin of Scythia during Mesozoic back-arc rifting and initial opening of the Greater Caucasus Basin [e.g., *Kazmin et al.*, 2000; *Zonenshain et al.*, 1990]. Thus, the presence of these blocks within the Lesser Caucasus explains the apparent north-domain signature in some samples on the southern side of the inferred suture zone. Specifically, the Dzirula Massif contains Variscan-aged zircons [e.g. *Mayringer et al.*, 2011], and is inferred by *Vincent et al.* [2013] to have served as a local source for both detrital zircon sample WG95/1 and three additional sandstone provenance samples (CG27/1, WG105/1, WG77/1) (Figure 6).

The presence of samples in the southernmost Greater Caucasus with south-domain provenance affinity (i.e., samples SW-GC and SE-GC and the 170 Ma peak in Inguri and Kumuk sediments) suggests that the Jurassic- to Eocene-aged island arc complex in the Lesser Caucasus now extends beneath the Cenozoic foreland basin cover of the Rioni, Kartli, and Kura basins as a large composite terrane, slivers of which are now exposed in south-directed thrust sheets along the southern margin of the Greater Caucasus. This configuration is supported by whole-sediment, major- and trace-element geochemical analyses, which indicate that volcaniclastic samples of the Mesozoic Vandam terrane in the southeastern Greater Caucasus of Azerbaijan are geochemically indistinguishable from modern sediment in rivers draining the southeastern Lesser Caucasus [*Forte*, 2012]. This correlation is also supported by the similarity between

Jurassic and Cretaceous aged volcanic rocks in the Vandam and those in deep wells within the Kura Basin [e.g., *Agabekov and Moshashvili*, 1978; *Shikalibeily et al.*, 1988].

5.4 Reconciling Pre-Bajocian (~170 Ma) Mixing of Sources

A peak of ~170 Ma grains is present in all samples analyzed in this study except for NW-GC, deposition of which predates this time, as well as 6 of the 9 previously reported samples: the Bajocian sandstone from the northeastern Greater Caucasus (GC41) [*Allen et al.*, 2006], Oligocene (WG95/1, WC99/3) and Miocene sandstones (WG66c/2, WC193/1) [*Vincent et al.*, 2013], as well as the modern Volga [*Wang et al.*, 2011] (Figure 5). Grains of this age appear to be an important component of the southern (Lesser Caucasus) domain, based on their abundance in the Tovuz and Kura River sediments and in samples associated with the Vandam (SE-GC, Kumuk), which is likely part of the Lesser Caucasus arc now incorporated into the Greater Caucasus as noted above. Significant Middle Jurassic arc volcanism has been reported in the Lesser Caucasus [e.g., *Sosson et al.*, 2010]. Amphibole and muscovite $^{40}Ar/^{39}Ar$ ages of 166-167 Ma have been reported for a single metamorphic block inferred to have rapidly exhumed by extension within the Lesser Caucasus arc prior to deposition within Upper Cretaceous subduction-related flysch within the IAESA suture [*Rolland et al.*, 2011]. Because of the predominance of ~170 Ma material in the Lesser Caucasus, the presence of this peak in samples north of the inferred suture zone (NE-GC, GC41, WC99/3, WC193/1, and Volga) is potentially problematic.

We interpret the occurrence of ~170 Ma grains in Mesozoic sandstones north of the suture zone (NE-GC and GC41) to indicate that the Greater Caucasus Basin was still relatively narrow at the time of their deposition. A more extreme interpretation is that opening of the Greater Caucasus Basin had not yet started, although we infer that extensive Middle Jurassic mafic dikes mapped within the crystalline basement of the Greater Caucasus [*Gubkina and Ermakov*, 1989] likely indicate that rifting was underway by this time. A narrow basin would have allowed for depositional transport into the northern domain of material sourced from the southern domain during the early stages of rifting (e.g., Figure 6). This transport most likely resulted from either primary northward air fall from the Lesser Caucasus arc or ~170 Ma volcanism on both sides of the back-arc basin as it was opening. Depositional exchange across the basin via far-travelled turbidites is less likely because it seems to predict north-domain grains in sample SE-GC that are not observed. Paleocurrent analysis could help to distinguish between these ideas, but we are unaware of such data. Small numbers of grains (< 3) of this age in Oligocene (early Maikop; WC99/3, Sochi) and Mio-Pliocene (Kimmerian; WC139/1, Taman) sandstone likely reflect either recycling of 170 Ma grains sourced from Mesozoic sediments in the northern domain that had been affected by Mesozoic sediment exchange during incipient rifting, or input of sediment from the southern domain during the later stages of Cenozoic basin closure, after the basin size had been significantly reduced. The origin of the single ~170 Ma grain in the Volga sample remains cryptic. Samples in the

southern domain contain the ~170 Ma peak because they are part of, or were sourced from the southern domain. Such samples include those from thrust sheets of S-domain rocks incorporated into the southern portion of the Greater Caucasus thrust belt (e.g., SE-GC, SW-GC, WG95/1, WG66c/2) and modern rivers crossing those sheets (Inguri, Kumuk), as well as modern rivers draining the southern domain (Tovuz, Kura).

5.5 Modern Rivers

Detrital zircon age spectra from modern sediments in the Inguri and Kumuk rivers, which drain the southern flank of the Greater Caucasus, contain both north- and south-domain components (Figure 5) and thus suggest mixing of north and south-domain provenance, although the overlap is not sufficient to appear in the Likeness values. Such mixing is expected because their catchments cross the Greater Caucasus thrust belt and thus the inferred suture zone (Figures 2a and 6). In contrast, those from the Kura and Tovuz, which drain the northern flank of the Lesser Caucasus, show derivation exclusively from the southern source. The catchment above the Tovuz River sample is located entirely south of the inferred suture zone and within the Lesser Caucasus. As expected, it shows a predominantly south-domain signature, with peaks dominated by Jurassic-Cretaceous aged zircons (Figure 5a). The small number of older grains in this sample likely reflects recycling from sediments originally containing material derived from Variscan basement in the Dzirula, Khrami, or Loki blocks, or Proterozoic basement in the Dzarkuniatz Massif (Figure 2a). The catchment above the Kura River sample is

primarily within Eocene-aged volcanic and volcaniclastic rocks in the Achara-Trialet zone [*Banks et al.*, 1997], and this sample is overwhelmingly represented by Oligocene-Eocene age zircons. Significant peaks at ~6-9 Ma reflect derivation from Mio-Pliocene volcanic rocks in eastern Anatolia [*Aldanmaz et al.*, 2000; *Keskin et al.*, 1998; *Pearce et al.*, 1990] while another at ~320 Ma indicates contribution from the Dzirula Massif, the east side of which lies within the sampled catchment. The ~320 Ma peak seems to be fairly diagnostic of Dzirula.

Modern Russian rivers draining the East European Craton and Scythian Platform are dominated by Precambrian ages, with secondary Paleozoic components (Figure 5a) [*Allen et al.*, 2006; *Safonova et al.*, 2010; *Wang et al.*, 2011]. As previously noted [e.g., *Vincent et al.*, 2013], the general lack of Precambrian grains in most samples from the Caucasus region indicates that the East European Craton was not a significant sediment source during Mesozoic opening of the Greater Caucasus Basin or its Cenozoic closure. These older grains are seen in Oligo-Miocene sandstones samples on the Taman peninsula (WC139/1), in the foreland basin on the north side of the Greater Caucasus (ILN#3_700), near Sochi (WC99/3) and one sample in western Georgia (WG66c/2), consistent with the inferred positions of these samples either north of, or within the northern porting of, the Greater Caucasus Basin prior to and during its closure.

5.6 Other Provenance Data

Below (Section 6.1), we infer that the Greater Caucasus Basin was likely on the order of ~350-400 km wide prior to Cenozoic closure. This differs from previous interpretations of a relatively narrow Paleogene transtensional basin [e.g., *Vincent et al.*, 2014], in which sediments were locally derived [e.g., *Vincent et al.*, 2013; *Vincent et al.*, 2007]. The key difference between the relict-ocean and transtensional basin models is in the latest Mesozoic to Paleogene paleogeography (Figure 6). Specifically, the existence of a large (~350-400 km wide) relict back-arc basin would be contradicted by Paleocene- to Eocene-aged deposits in the Greater Caucasus north of the inferred suture zone showing derivation from the Lesser Caucasus, or similarly aged sediments south of the inferred suture zone showing derivation from the Variscan basement and associated Paleozoic sediments now exposed in the core of the western Greater Caucasus. However, this latter test is complicated by Variscan basement of the Dzirula, Loki, and Khrami Massifs within the Lesser Caucasus provenance domain.

A number of provenance analyses have been reported from the central and western Greater Caucasus between 36°E and 46°E, including compositions of sandstones, their constituent rock fragments, and heavy mineral fractions, as well as analyses of palynomorphs and detrital zircon ages [*Vezzoli et al.*, 2014; *Vincent et al.*, 2014; *Vincent et al.*, 2013; *Vincent et al.*, 2007]. Most of these data do not bear directly upon the Paleogene paleogeography of the Greater Caucasus Basin because they have depositional

ages that significantly postdate the time of inferred maximum basin extent (Figure 6) and/or are from areas outside the closed relict back-arc basin (i.e., west of 41.5°E, Figure 2). Locations of key provenance analyses discussed below are listed in Table S1 and shown in Figures 2 and S1, and include sandstone compositions (Figure S4a), detrital grain compositions (Figure S4b) and heavy mineral analyses (Figure S4c) reproduced from *Vincent et al.* [2013].

Except for samples along the northern edge of the Lesser Caucasus, all of the provenance samples east of 41.5°E basin now lie structurally above south-directed thrusts [e.g., *Banks et al.*, 1997; *Philip et al.*, 1989] that formed during basin closure and subsequent collision between the Variscan basement of the Greater Caucasus to the north and the dominantly Mesozoic-Cenozoic Lesser Caucasus arc to the south. As a result, their positions within the basin at the time of deposition are unknown. For the few older Cenozoic samples within this zone, the most diagnostic provenance signatures are the detrital zircon spectra and sandstone detrital-grain compositions, particularly the relative abundances of plutonic and metamorphic rock fragments, inferred to be sourced from the Variscan basement of either the Greater Caucasus or the Dzirula massif [*Vincent et al.*, 2014; *Vincent et al.*, 2013]. In detail, only 13 reported samples east of 41.5°E are old enough to potentially bear upon the Paleogene paleogeography, with 5 Oligocene (33.9 to 23.0 Ma) and 8 early Miocene (23.0 to 16.0 Ma) aged samples. Of these 13, only 8 have reported sandstone point-count results (Figure S4a). Of those 8 samples, 5 show >3%

plutonic and metamorphic rock fragments (Figure S4b), including detrital zircon sample WG95/1. However, this sample and 2 others in this age group (CG27/1, WG105/1) are inferred to have been locally sourced from the Dzirula massif [*Vincent et al.*, 2014; *Vincent et al.*, 2013]. As noted above (Section 5.3), it appears that during the Paleogene the Dzirula massif served as a localized source of sediment of apparent north-domain affinity within the southern domain. Therefore, the only provenance data potentially linking the northern and southern domains in the key time interval are the compositions of detrital grains in two samples (WG28c/1 Maykopian/Late Chattian; WG27/4, Maykopian/Aquitanian-Burdigalian), both of which are from the Chanis River section along the southern margin of the Greater Caucasus (Figures 2a, 6, and S4b).

Based on its structural position within the Caucasus thrust belt, age, and provenance, we interpret the Chanis River section to have been deposited within the interior of the basin, tens to potentially hundreds of kilometers south of the core of the Greater Caucasus, and to cover the period of time during which the basin started to close and then progressively narrowed. As noted by *Vincent et al.* [2007], the Chanis River section records onset of sedimentation sourced from the Greater Caucasus in Late Oligocene (Maykopian/Late Chattian) time (e.g., ~25 Ma). The base of the section comprises Late Eocene to Early Oligocene hemipelagic mudstone; sandstone (e.g., WG28b/3 and WG28c/1) first appears in the Late Oligocene as thinly bedded deposits from low-density (i.e., distal) turbidites [*Vincent et al.*, 2014; *Vincent et al.*, 2007]. The

lowest sandstone sample in the section, WG28b/3 [sample A1 in *Vincent et al.*, 2007] has < 1% plutonic and metamorphic clasts and thus lacks a strong Greater Caucasus provenance signature. However, plutonic and metamorphic grains inferred to be sourced from the Greater Caucasus crystalline core had appeared by the time sample WG28c/1 was deposited in Late Chattian (Maykopian) time and continue in Aquitanian-Burdigalian (Maykopian)-aged sample WG27/4 [sample A3 in *Vincent et al.*, 2007]. The Chanis River section also contains populations of detrital apatites with fission-track ages of 34 ± 6 Ma (WG28c/5; A2) and 31 ± 3 Ma (WG27/4; A3), south-directed paleocurrent indicators, and abundant reworked nanofossils that are dominated by Eocene forms near the base but increasing proportions of Cretaceous forms up section [*Vincent et al.*, 2014; *Vincent et al.*, 2007]. In general, the timing of a provenance shift recorded by any given sedimentary section depends on the position of the section in the basin [e.g., *DeCelles and Giles*, 1996], but this position is unknown for the Chanis River section. However, based on the distal depositional environments and numerous thrusts between the section and inferred sources in the core of the Greater Caucasus [e.g., *Adamia et al.*, 2011; *Banks et al.*, 1997], we infer that the section was deposited well out in the Greater Caucasus Basin and records long-transport sediments that were sourced from thrust sheets within the Greater Caucasus to the north.

If basin closure had started by ~35 Ma, as inferred from the detrital apatite fission track ages reported by *Vincent et al.* [2007], then the provenance transition in the Chanis

River section at ~25 Ma dates from a time when the basin had partially closed. Specifically, the basin may have been on the order of ~250 km wide at the time of late Oligocene (~25 Ma) deposition of samples WG28b/3 and WG28c/1, assuming an original width of ~350 km, based on the modern Black Sea and South Caspian basins as analogs, onset of closure at ~35 Ma, based on the detrital apatite fission track ages reported by *Vincent et al.* [2007], and a time-averaged closure rate of ~10 mm/yr, based on the similarity of geologic and geodetic rates of convergence between the Lesser and Greater Caucasus over the past several million years [*Forte et al.*, 2010; *Forte et al.*, 2013; *Reilinger et al.*, 2006].

Although sparse, the currently available detrital zircon and provenance data from samples east of 41.5°E constrain significant depositional mixing across the Greater Caucasus Basin to be middle Miocene or younger. Sample SW-GC, with a maximum depositional age of ~27 Ma, is dominated by peaks of south-domain affinity. Likewise, sample WG66c/2, with a Langhian (Chokrakian) depositional age, lies in the middle of the suture zone, and is dominated by Variscan and EEC provenance peaks, consistent with expected deposition south of a growing Greater Caucasus range. Both samples suggest the provenance domains remained largely distinct up to the time of their deposition, although they also contain hints of depositional exchange in the form of a few, single-grain peaks of north- or south-domain affinity in SW-GC or WG66c/2, respectively. In contrast, younger provenance samples WG22/5, Tortonian (Middle

Sarmatian) and WG15/5, Tortonian-Messinian (Meotian), from south of the suture zone (Figure S1) contain >3% plutonic and metamorphic grains, and thus appear to attest to transport of sediments sourced from the Greater Caucasus across the suture zone by the time of their deposition.

6. Tectonic Implications

6.1 Size of Subducted Greater Caucasus Basin

The contrast in provenance across the Greater Caucasus Basin indicates that an intervening ocean basin analogous to the eastern Black Sea or South Caspian Basin separated Mesozoic sandstones studied here at the time of their deposition, preventing exchange of sediments sourced from opposite sides of the basin. Collision of the South Armenian block with the Lesser Caucasus occurred in either the Late Cretaceous [*Rolland et al.*, 2011] or Paleocene [*Sosson et al.*, 2010], suggesting the Greater Caucasus Basin and southern branch(es) of Neotethys were the principal oceanic basins between the Arabian and Eurasian continents after this time. Several factors imply the Greater Caucasus basin was likely ~350-400 km wide at its maximum extent in the late Mesozoic to early Cenozoic. Paleomagnetic data from the ATA block indicate the basin was no more than 1000 km across in Late Cretaceous time [*Meijers et al.*, 2015]. (A) Both the eastern Black Sea and South Caspian Basin are presently ~350 km wide perpendicular to the strike of the Greater Caucasus. Both were larger prior to Cenozoic shortening on

thrusts along the northeastern margin of the Black Sea [*Munteanu et al.*, 2011; *Nikishin et al.*, 2010; *Robinson et al.*, 1996] or via both northward subduction of the South Caspian beneath the Apsheron Sill [*Allen et al.*, 2002; *Jackson et al.*, 2002; *Mangino and Priestley*, 1998; *Priestley et al.*, 1994] and south-directed underthrusting beneath the Alborz [*Ballato et al.*, 2015]. (B) Large modern turbidite systems are known to travel up to 500 km [*Elmore et al.*, 1979; *Piper and Aksu*, 1987; *Talling et al.*, 2007; *Wynn et al.*, 2002] suggesting the basin was of similar scale to preclude depositional exchange. (C) Finally, Eocene magmatic rocks of the Pontide-Lesser Caucasus arc are deflected northward by up to 300 km between 41.5° and 48.5°E relative to their positions to the west and east (Figure 7) defining an orocline [*Bazhenov and Burtman*, 2002; *Meijers et al.*, 2016 in press]. New and compiled paleomagnetic data suggest that most of this curvature developed after the Paleocene, although 40°± 25° of bending appears to predate the Late Cretaceous [*Meijers et al.*, 2016 in press]. In detail, *Meijers et al.* [2016 in press] perform strike tests on the Lesser Caucasus orocline using a mixture of new measurements and previously reported data from the International Association of Geomagnetism and Aeronomy Global Paleomagnetic Database (GPMDB) to explore the timing of orocline formation. Based on these data, they conclude progressive orocline formation, with some pre-existing curvature (40 ± 25%) developed prior to the Late Cretaceous, additional (~10%) bending after the Paleocene but before the Middle Eocene, and a 48 ± 13% of final rotation after the Eocene (and most likely before Late Miocene).

However, as the authors note, the strike tests for the Late Cretaceous-Paleocene and Eocene data are indistinguishable at 95% uncertainty. Thus, the inferred Paleocene-Eocene phase of bending could actually be post-Eocene (i.e., ~60% of the total bending). Thus, within uncertainty these data permit as much as 75% of the oroclinal bending to be post-Eocene. Importantly, the results of the strike tests are also highly sensitive to the assumed regional strike for the individual measurement sites, which is not well determined. In summary, the uncertainty in the existing paleomagnetic data both permit a wide range of interpretations of the timing of oroclinal bending and highlight the need for additional data, although the rocks necessary to further clarify the history of orocline formation may simply not exist, as discussed by *Meijers et al.* [2016 in press].

Our reconstruction (Figure 8) schematically accounts for some pre-Eocene oroclinal bending, but attributes most to deformation associated with closure of the Greater Caucasus basin following Eocene collision of Arabia with the Bitlis-Pötürge massif and closure of the Bitlis-Zagros suture. This model requires major structural systems on the margins of the orocline to accommodate northward migration of the Lesser Caucasus and Talysh relative to the Black and Caspian Seas. In general, such migration can be accommodated by either strike-slip transfer faults, in the case of a non-rotational orocline, or thrusts, in the case of a rotational bend [e.g., *Cowgill*, 2010 and references therein]. Combinations of such systems are also possible. The West Caspian fault [*Allen et al.*, 2003] may play such a role on the east flank of the orocline. The

geometry of the Bitlis-Zagros suture reflects the integrated effects of post-collisional deformation north of the suture but does not preclude significant along-strike variability in the mechanisms by which this northward motion of Arabia relative to Eurasia was absorbed. Such convergence has been absorbed by westward extrusion of Anatolia west of ~41°E [e.g., *McKenzie*, 1972], closure of the Greater Caucasus Basin and shortening within the EAAC in the central third of the collision, and shortening (± strike-slip faulting) in the Zagros [*Talebian and Jackson*, 2002], Alborz [*Axen et al.*, 2001; *Ballato et al.*, 2011; *Ballato et al.*, 2013; *Guest et al.*, 2006], and Apsheron Sill [e.g., *Allen et al.*, 2002] east of ~48°E. We speculate that the Black and South Caspian relict basins are still present in the western and eastern thirds of the collision because both regions are bound to the south by subduction zones in Cyprus and the Makran, which have allowed for lateral extrusion of intervening crust.

Cenozoic closure of a 350-400 km wide basin falls well within the known amount of post-collisional plate convergence. Between 35 and 5 Ma, total convergence between Arabia and Eurasia was ~800 km (Figure 1b) [*Hatzfeld and Molnar*, 2010; *McQuarrie et al.*, 2003], the orogen-perpendicular component of which would have been less than this amount, but still in excess of 400 km. Some previous paleomagnetic studies from the region indicate that the Lesser Caucasus have moved north by as much as 10° of latitude (>1000 km) since Eocene time [e.g., *Bazhenov and Burtman*, 1989; *Bazhenov and Burtman*, 2002], although paleomagnetic data from the region are complex, of variable

quality, with evidence of inclination shallowing or insufficient averaging of secular variation in some cases [*Meijers et al.*, 2016 in press]. Thus, the timing and magnitude of such a translation remain to be firmly established. If confirmed, however, this interpretation of the paleomagnetic data is consistent with a basin hundreds of kilometers wide.

Closure of the basin appears to have been accommodated by northward subduction of basin crust beneath the Greater Caucasus. Subduction beneath the Greater Caucasus has been argued for some time based on seismicity [*Khain and Lobkovskiy*, 1994; *Khalilov et al.*, 1987]. *Mellors et al.* [2012] documented subcrustal (depth > 50 km) earthquakes beneath the range with a maximum depth of 158 ± 4km, and *Skolbeltsyn et al.* [2014] identified a high-velocity shear wave anomaly extending to a depth of ~250 km in the same region. *Mumladze et al.* [2015] used hypocenter locations from regional catalogs to identify an inferred Wadati-Benioff zone east of 45°E beneath the central and eastern Greater Caucasus. This zone of seismicity dips ~40° to a maximum resolved depth of ~158 km, implying a slab length of 130 – 280 km [*Mumladze et al.*, 2015 and supplement], suggesting subduction of at least this length of crust. The down-dip extent of seismicity is only a minimum constraint on the amount of subduction, because the slab can continue to greater depths but be too warm to support brittle failure [*Molnar et al.*, 1979]. The observed down-dip length of seismicity is consistent with that expected for subduction of ~180 Myr old lithosphere at a rate of ~10 mm/yr [*Molnar et al.*, 1979]. The

absence of subcrustal seismicity west of 45°E suggests the slab has detached here, and a possible tear in the slab to the east of 45°E suggests such detachment may be propagating eastward [*Mumladze et al.*, 2015]. Thus, subducted slabs provide only ephemeral evidence of basin closure.

6.2 Two Stage Collisional History

When integrated with recent thermochronologic data and prior work in the orogen, the detrital zircon data presented here indicate the Arabia-Eurasia collision occurred in two stages (Figure 8), similar to a recent proposal for the India-Eurasia collision [*van Hinsbergen et al.*, 2012]. A two-stage collision was also inferred by *Ballato et al.* [2011] and has significant implications regarding the mechanical behavior of the orogen.

In the first phase (soft collision), Arabia collided with the southern margin of the East Anatolia Accretionary Complex (Figure 2) and closed the Bitlis-Zagros suture, at which point shortening rates in the Bitlis-Zagros suture zone decreased as the locus of convergence jumped to the northern margin of the Greater Caucasus Basin, which started to close by north-directed subduction of the basin crust (Figure 8). The distance between the Bitlis-Zagros suture and the new shortening zone was likely at least ~1000 km, based on the combination of the inferred basin width (~350-400 km) and the present distance between the Bitlis-Zagros and Greater Caucasus suture zones (~700 km); accounting for post-collisional shortening within the Lesser Caucasus and East Anatolian Plateau adds to

this distance. Shortening of the Greater Caucasus basin led to the initiation of deformation and exhumation of thrust sheets in the Greater Caucasus starting in late Eocene to early Oligocene time at rates of a few °C/Ma, as indicated by consistent thermochronologic data from transects north of the inferred suture zone in the western, central, and eastern Greater Caucasus [*Avdeev*, 2011; *Avdeev and Niemi*, 2011; *Vincent et al.*, 2011]. The first-order shape of the Ab-Eu orogenic belt appears to result from closure of this basin: between 41° and 48°E, subduction of the Greater Caucasus relict basin allowed Arabia to indent northward, contributing to the deflection of the Pontide-Lesser Caucasus arc (Figure 2b), via oroclinal bending (Figure 7). To the west, convergence was absorbed by west-directed lateral extrusion of Anatolia on the conjugate North and East Anatolian faults [*McKenzie*, 1972], whereas to the East in Iran, oblique convergence was partitioned into dextral slip on the Main Recent Fault [*Talebian and Jackson*, 2002] and shortening in the Zagros [e.g., *Agard et al.*, 2005; *Berberian*, 1995], with additional shortening in the Alborz [*Axen et al.*, 2001; *Ballato et al.*, 2015; *Guest et al.*, 2006], and possibly the Apsheron sill [*Allen et al.*, 2002] (Figure 2b).

The second phase of hard collision started when the Greater Caucasus relict back-arc basin finally closed, leading to collision between its northern and southern margins in late Miocene or early Pliocene time, when exhumation rates increased by as much as a factor of ten in the central and eastern Greater Caucasus (Figure 8) [*Avdeev*, 2011; *Avdeev and Niemi*, 2011]. The timing and significance of this transition are

consistent with a regional tectonic reorganization of the Arabia-Eurasia collision zone at ~ 5 Ma [*Allen et al.*, 2004; *McQuarrie et al.*, 2003; *Westaway*, 1994]. Data presented here and elsewhere [*Avdeev*, 2011; *Forte*, 2012] indicate that this collision was between the arc basement of the Lesser Caucasus to the south and Variscan basement along the southern edge of the Scythian platform of Eurasia to the north, and resulted in incorporation of Lesser Caucasus basement into thrust sheets in the southern Greater Caucasus. The Pliocene increase in exhumation rate has not been reported from the northwestern Greater Caucasus [*Vincent et al.*, 2011], probably because the apatite fission-track methodology employed by *Vincent et al.* [2011] was not sensitive to the rate change recorded by the lower-temperature (U-Th)/He methodology used by *Avdeev and Niemi* [2011]. This apparent discrepancy may also stem from the differences in the structural and geomorphic settings between the two studies. Most of the samples investigated by *Vincent et al.* [2011] are from the low relief southern flank of the range. The magnitudes and rates of exhumation are expected to be slow in this area, assuming that topography and long term uplift rate are correlated, which appears to be the case in the Greater Caucasus [*Forte et al.*, 2016]. Where *Vincent et al.* [2011] sample high relief areas comparable to those studied by *Avdeev and Niemi* [2011], the AFT ages are similarly young (e.g., an AFT age of 2.5 ± 0.6 Ma from north of the MCT).

Since the onset of collision, deformation has propagated southwards into the foreland basin. For example, between 47ºE and 48ºE, the deformation front propagated

into the foreland basin at ~2 - 1.5 Ma [*Forte et al.*, 2013], focusing shortening within the Kura fold-thrust belt [*Forte et al.*, 2010]. Since formation, this foreland thrust-belt has absorbed almost all convergence between the Lesser and Greater Caucasus (80-100%) and most (~60%) of the orogen-perpendicular shortening between Arabia and Eurasia. This contrasts with prior work, which inferred that most present-day shortening in the Caucasus region is localized on thrust systems at the southern topographic front of the Greater Caucasus [e.g. *Allen et al.*, 2004; *Philip et al.*, 1989; *Reilinger et al.*, 2006].

6.3 Implications for Balancing Shortening Deficits

Relict basin closure has likely occurred relatively frequently throughout Earth history. Most of the modern Pacific basin is fringed with back-arc basins attesting to the common occurrence of such features during protracted subduction and terrane accretion within long-lived ocean basins and prior to their closure. Even in the absence of back arc basins, the margins of colliding continents are typically irregular [e.g., *Dewey*, 1977; *Dewey and Burke*, 1974], leading to the formation of remnant ocean basins during collision [*Graham et al.*, 1975; *Ingersoll et al.*, 1995] such as the Bay of Bengal. Thus, relict-basin closure is likely common during the transition from subduction to soft continental collision to, ultimately, hard continental collision .

Relict basin closure such as that described here for the Greater Caucasus has significant implications regarding the mechanics of collisional orogens and the dynamics of plate motions. One implication is that relict-basin closure can accommodate significant

plate convergence with minimal upper-crustal shortening because convergence is absorbed as subduction and/or underthrusting. In subduction zones, total plate convergence typically exceeds the amount of crustal shortening by a large fraction. However, closure of a large ocean basin typically leaves other signatures in the geologic record, such as accretionary complexes, blueschist-facies metamorphic belts, magmatic arcs, or juxtaposition of rocks from dispersed paleolatitudes or faunal zones. In contrast, subduction of relatively small (250-500 km wide) ocean basins is likely to be hard to detect because it primarily occurs as shortening along structural systems that are easily hidden within flysch or slate belts, e.g. the large deposits of flysch within the Greater Caucasus. The age and nature of the back-arc basin crust may play an important role in the geologic record of basin closure, with subduction of old/cold oceanic lithosphere perhaps being more obscure than that of young/warm or transitional lithosphere, the buoyancy of which should result in greater accretion and upper-plate deformation relative to old/cold oceanic lithosphere. The obscurity of such shortening is compounded in collisional orogens with protracted histories of post-collisional convergence, in which younger deformation obscures or overprints early strain. Within ancient orogens, closed relict basins may be expressed as flysch or slate belts, and the Greater Caucasus may serve as a modern analog for the development of such tectonic domains. Thus, an implication of the present study is that accretion of such slate belts may have

accommodated hundreds of kilometers of shortening via subduction of their underlying oceanic basement.

Although relict-basin closure may help reconcile deficits of upper-crustal shortening relative to post-collisional convergence, it should be noted that there is no a priori reason to expect such balance. As Figure 9 shows, there is no unique relationship between upper crustal shortening (S), plate convergence (C), and length of subducted slab (L), with S < L, S = L and S > L all possible. To explain, we first differentiate two basic types of upper crustal shortening. In accretionary shortening (S_A), material is transferred into the orogen from either plate during subduction, and slip on the thrust or shear zone underlying each accreted sheet feeds into displacement of the subducted slab relative to the upper plate (Figure 9). The structural link is via the basal decollement beneath the orogen, either along the subduction thrust or a linked backthrust, in the case of a bivergent [*Willett et al.,* 1993] or floating orogen [*Oldow et al.,* 1990]. In thickening shortening (S_T), there is no such subduction, so that upper-crustal shortening is matched by a corresponding thickening of the underlying crust and mantle lithosphere beneath the orogen (Figure 9). Simple volume balancing and the above definitions lead to three end-member mechanisms that can accommodate post-collisional plate convergence within a collisional orogen (Figure 9). The first (Figure 9a) is subduction with neither accretion ($S_A = 0$) nor upper-plate shortening ($S_T = 0$). In this case, upper crustal shortening is zero (S = 0) and the length of the subducted slab, barring removal or detachment of any

portion of the slab, equals the magnitude of plate convergence (L = C). A second end member is accretionary shortening, in which all convergence is accompanied by accretion during subduction (Figure 9b). In this case, $S = S_A = L = C$. A third possibility is "pure-shear" shortening of the orogen [e.g., *Allmendinger and Gubbels*, 1996], where the upper crust shortens from convergence and crustal thickening without associated subduction. In this case, $S = S_T = C$, and there is no slab or accretion, so $L = S_A = 0$ (Figure 9c). Attempts to balance crustal shortening with plate convergence implicitly assume either the second or third end-member scenarios, or some combination of the two.

The most general scenario is one where all three processes operate either simultaneously or at different times during collision. In this most general, and we argue realistic, case, there is no unique relationship between S and L. For example, $S < L$ is expected for an orogen with subduction but minimal accretion. Likewise, an orogen with minimal subduction but significant post-collisional lithospheric thickening can have $S > L$. The expected case of balanced shortening and convergence ($S = C$) occurs only when there is either no subduction ($L = 0$), or when all subduction is recorded by accretion ($S_A = L$). Thus, $S < L$, $S > L$, and $S = L$ are all possible, depending on the relative contributions of the different end-members.

In the Greater Caucasus, restoration of the preliminary cross section in Figure 4 from the western end of the range yields a minimum estimate of upper-crustal shortening of ~130 km, although ongoing work indicates that estimate is too low [e.g., *Trexler et al.*,

2015] . At the eastern end of the range, the observed length of subducted slab is 130 to 280 km [*Mumladze et al.*, 2015], although the true length could be larger if the slab is too warm to support brittle failure at depth [e.g., *Molnar et al.*, 1979]. In the context of Figure 9, these numbers could indicate convergence within the Greater Caucasus of at least 260 km, in the case where L > 130 km reflects subduction without accretion (Figure 9a), combined with pure-shear shortening to produce S ~130 km (Figure 9c). Alternatively, convergence could be only ~130 km, in the case of complete accretion & upper-plate shortening to produce S = L ~130 km.

6.4 Implications for Deceleration of Plate Motion

It also appears that relict-basin closure can delay deceleration of plate motion. Collisions change the balance of forces acting on a subducting plate sufficiently to slow plate motions [*Dewey et al.*, 1989; *Molnar and Lyon-Caen*, 1988; *Patriat and Achache*, 1984]. In the Indo-Asian collision, which serves as the type example of this process, there has been a significant (40%) deceleration in the rate of plate convergence since the onset of the collision [e.g., *Copley et al.*, 2010; *Molnar and Stock*, 2009], although the mechanism underlying this change remains disputed. One idea is that an increase of gravitational potential energy due to crustal thickening and formation of an orogenic plateau resists plate convergence and slows subduction [*Austermann and Iaffaldano*, 2013; *Copley et al.*, 2010; *Flesch et al.*, 2001; *Molnar and Lyon-Caen*, 1988; *Molnar and Stock*, 2009]. Another possibility is that convergence slowed due to a reduction in the

slab-pull force following slab breakoff [*Capitanio and Replumaz*, 2013] or an increase in buoyancy of the subducting slab due to subduction of continental lithosphere along the leading edge of the incoming continent [*Capitanio et al.*, 2010]. More recently, it has been proposed that post-collisional convergence rates slow exponentially because of constant viscous resistance to plate motion by the upper-plate continental mantle lithosphere [*Clark*, 2012].

In contrast to Tibet, the Ab-Eu collision appears to show a significant delay in the onset of both deceleration of plate motion [*Austermann and Iaffaldano*, 2013] and widespread upper plate deformation and sedimentation [*Ballato et al.*, 2011]. Deceleration and onset of widespread deformation post-date by ~30 to 15 Myr the onset of collision between Arabia and the southern margin of Eurasia along the Bitlis-Zagros suture in late Eocene to early Oligocene time [*Agard et al.*, 2005; *Allen and Armstrong*, 2008; *Ballato et al.*, 2011; *Boulton and Robertson*, 2007; *Hempton*, 1985; 1987; *Rolland et al.*, 2012; *Yilmaz*, 1993]. Closure of an old, cold relict back-arc basin explains this marked difference in the mechanical behavior of the two orogens. In particular, we argue that the northward motion of Arabia was not significantly impeded at the onset of Eocene to early Oligocene collision because deformation was able to jump ~1000 km northward into the interior of the overriding plate and continue at the same pace by consumption of the relict basin. Closure of the relict basin led to basement collision between the Greater and Lesser Caucasus and incorporation of the Lesser Caucasus basement into the Greater

Caucasus orogenic wedge. Most significantly, this transition from soft to hard collision changed the force balance sufficiently to trigger structural reorganization of the Ab-Eu collision zone as a whole. A tectonic reorganization at ~5 Ma has been recognized across much of the collision zone [*Allen et al.*, 2004; *McQuarrie et al.*, 2003; *Westaway*, 1994]. We attribute much of this reorganization to ~5 Ma collision between the Greater and Lesser Caucasus basements at the end of relict-basin closure, when the basement of the Lesser Caucasus began underthrusting that of the Greater Caucasus.

Although the Greater Caucasus provide an example of relict basin closure in the upper plate, closure of a relict basin in the lower plate is equally capable of accommodating post-collisional convergence with minimal crustal shortening. For example, *van Hinsbergen et al.* [2012] propose a two-stage model of the Indo-Asian collision, in which post-collisional convergence was first absorbed by subduction of the largely oceanic Greater India Basin during soft collision. Cenozoic closure of this Cretaceous extensional basin eventually resulted in collision of the Indian crust with the Tethyan Himalaya and Eurasia to the north, leading to the onset of hard collision at ~25-20 Ma. From this we infer that the physical and rheological properties of the colliding lithosphere likely play a fundamental role in modulating post-collisional plate convergence rates, with lithosphere that is young and warm (e.g., Greater India Basin) producing more resistance during early collision than when it is old and cold (Greater

Caucasus Basin), subduction of which allows convergence to continue apace until the relict basin has been consumed.

7. Conclusions

The Greater Caucasus is characterized by distinct northern and southern provenance domains between 41.5° and 48°E, as indicated by new detrital zircon analyses of 8 samples (4 sandstone, 4 modern) integrated with prior provenance results. The northern domain, within the central and northern Greater Caucasus, is characterized by detrital zircon age spectra with broad distributions of Mesozoic to Precambrian grains and plutonic and metamorphic rock fragments that together characterize the Variscan basement along the southern margin of the Scythian Platform and East European Craton. The southern domain, within the southern margin of the Greater Caucasus and the Lesser Caucasus Mountains, is defined by age spectra in Mesozoic to early Cenozoic strata consisting almost exclusively of Mesozoic grains, with little to no contribution from the older Variscan or East European Craton sources, except for samples proximal to the Dzirula, Khrami, or Loki Massifs, a set of Variscan basement blocks of north-domain affinity within the southern domain.

The general lack of age overlap between the northern and southern provenance domains implies that during late Mesozoic to early Cenozoic time, the Greater Caucasus Basin was wide enough to largely prevent depositional exchange between them. Both the

widths of the analogous Black Sea and South Caspian Basin, and runout distances of modern turbidite systems suggests the basin could have been on the order of ~350 to 400 km wide.

We follow previous workers [e.g., *Zonenshain and Le Pichon*, 1986] in concluding that the Greater Caucasus formed by closure of a relict Mesozoic back-arc ocean basin. In Late Cretaceous to Paleocene time this basin was contiguous with the Black and Caspian Seas, and likely of similar width. Evidence of depositional exchange between the northern and southern areas in younger deposits (WG22/5 and WG15/5) suggests the width of the Greater Caucasus Basin had been significantly reduced by middle to late Miocene time.

Sediment provenance data [*Vincent et al.*, 2014; *Vincent et al.*, 2013; *Vincent et al.*, 2007] and thermochronologic data [*Avdeev*, 2011; *Avdeev and Niemi*, 2011; *Kral and Gurbanov*, 1996; *Vincent et al.*, 2011] together indicate shortening and exhumation in the Greater Caucasus started by ~35 Ma, which we infer to result from soft collision between Arabia and the Bitlis-Pötürge massif triggering initiation of subduction in the Greater Caucasus Basin at this time. The locus of Ab-Eu convergence jumped northward at ~35 Ma, and was absorbed between 41.5° and 48°E by subduction of the Greater Caucasus Basin and other similar basins to the south in eastern Anatolia. Eventual collision of the Lesser Caucasus with the Variscan margin of Scythia at ~5Ma led to hard collision,

kinematic reorganization within the collision zone, and a post 5 Ma deceleration in plate convergence rate.

Relict basin closure can significantly delay the deceleration in rates of plate motion because it delays the onset of hard collision. Thus, closure of the Greater Caucasus Basin provides an alternative explanation for the significant delay in Ab-Eu convergence rates following initial collision. Likewise, relict-basin closure provides a mechanism for reconciling deficits of upper crustal shortening relative to post-collisional plate convergence. Basin closure by subduction with minimal to no upper-plate shortening, provides an effective mechanism for hiding shortening within collisional orogens. Thus, upper plate shortening need not directly correspond to the amount of post-collisional plate convergence.

Outstanding problems include constraining the Late Cretaceous to Paleocene paleogeography of the Greater Caucasus Basin and how the Pontide-Lesser Caucasus domain continues eastward into Iran. Likewise, an updated plate circuit with both better constraints on Red Sea rifting and finer temporal resolution is essential for resolving the magnitudes, rates, and history of relative motions between the Arabian and Eurasian plates.

Acknowledgements

Data used in this study are reported in the supplement, figures, and references. Support for this work was provided by the National Science Foundation through EAR-Tectonics and the Office of International Science and Engineering under awards 0810285 and 1524631 to Cowgill and 0810067 and 1524304 to Niemi. We thank Yann Rolland and Paolo Ballato for their constructive and helpful reviews, which improved the paper. We also thank Tea Mumladze, Ana Menabde, Otto Tomadze, and David Kandelaki for assistance in the field, Sarah Roeske and the UCD microprobe facility for mount imaging, and George Gehrels, Mark Pecha, Dominique Giesler, Intan Yokelson, and Mauricio Ibanez-Mejia for assistance with U-Pb analyses at the Arizona LaserChron Center, which is supported by NSF-EAR grant 1338583. Cowgill thanks Kerry Sieh, Jean Philippe-Avouac, and the O.K. Earl Postdoctoral Program at the California Institute of Technology for supporting his initial work in the Arabia-Eurasia collision zone.

Figures

Figure 1:

(a) Comparison of crustal - shortening deficits in the Arabia - Eurasia and India - Eurasia collisions within the Alpine-Himalaya belt [modified from *van Hinsbergen et al.*, 2012]. Total bar height indicates amount of post-collisional plate convergence expected at the lower-plate reference points (locations approximated by stars). Green and blue bars

show amount of observed upper- and lower-plate crustal shortening, respectively. Red bars indicate apparent shortening deficits. Values for India - Eurasian collision are from *van Hinsbergen et al.* [2012]; convergence and shortening-deficit information for Arabia - Eurasia collision are from *Hatzfeld and Molnar* [2010] and *McQuarrie and van Hinsbergen* [2013]. White dots indicate detrital zircon samples of modern rivers draining East European Craton reported by *Wang et al.* [2011]. Base image is the World Imagery Basemap Layer from ESRI. (b) Plot showing distance Arabian reference point P1 (Figure 2b) traveled relative to Eurasia over time [after *Hatzfeld and Molnar*, 2010]. Numbers above line segments give incremental convergence rates (in mm/y). Gray box spans range of current estimates for age of onset of Ab-Eu collision; lower-left and upper-right corners indicate the maximum (~900 km) and minimum (~700 km) magnitudes of post-collisional Ab-Eu convergence, respectively. Arrows indicate the > 200 km difference (red arrow) between magnitude of post-collisional convergence (700 to 900 km, gray box) and estimated upper-plate shortening (~500 km, blue arrow) reported by *McQuarrie and van Hinsbergen* [, 2013]. (c) Plot of Ab-Eu convergence rate over time for reference point P2 (Figure 2b) [after *Austermann and Iaffaldano*, 2013]. Red lines with dashed confidence bounds are computed from a plate circuit, the point with error bars is determined from GPS geodesy. Note the ~30% decrease in Ab-Eu convergence rate over the last 5 Ma. Rates at ~5Ma differ between the two panels (i.e., 20 mm/yr in B and 30 mm/yr in C) because they were computed using different stages (and thus average over

different time intervals), reference points, and rotation poles [e.g., see details in *Austermann and Iaffaldano*, 2013; *McQuarrie et al.*, 2003].

Figure 2:

(a) Simplified tectonic map of Greater and Lesser Caucasus, showing locations of main structures and new U-Pb detrital zircon samples (diamonds: bedrock sandstone; stars: modern river sediment, with catchments delineated by black lines edged in white). Dots denote locations of previously reported detrital zircon [white fill, *Allen et al.*, 2006; *Vincent et al.*, 2013] and provenance analyses [gray fill, *Vincent et al.*, 2014; *Vincent et al.*, 2013; *Vincent et al.*, 2007] discussed in text; see Figure 6 for additional sample numbers. Fault geometries are simplified on northern margin of central Greater Caucasus and shown as north-directed thrusts; true geometries are south-directed backthrusts above a triangle zone at the leading edge of a generally north-directed thrust system [e.g., *Sobornov*, 1994; *Sobornov*, 1996]. MCT: Main Caucasus Thrust. Basement massifs: DM – Dzirula, KM – Khrami, LM – Loki, and DkM – Dzarkuniatz. Boxes indicate locations of cross sections in Figures 2c and 4. (b) Map of Arabia-Eurasia collision zone; black lines indicate major structural systems; red arrows show motion of Arabia relative to Eurasia from the 2010 GEODVEL model, with numbers indicating rates in mm/yr [*Argus et al.*, 2010]; red dots are reference points for plots of plate convergence (P1) and rate (P2) over time (see Figure 1); white dots are published detrital zircon samples from Oligo-Pliocene sandstone [*Vincent et al.*, 2013]; dashed yellow lines indicate Bitlis and

Izmir-Ankara-Erzincan-Sevan-Akera (IAESA) sutures [*Rolland et al.*, 2012] bounding the ATA (Anatolide-Tauride-Armenian) block, which contains the South Armenian Block and is bound to the south by the East Anatolian Accretionary Complex (EAAC). WCF: West Caspian Fault [*Allen et al.*, 2003]. (c) North-dipping zone of earthquakes extending to ~160 km beneath the Greater Caucasus indicates subducted basement of the relict ocean basin. Panels a-b after *Forte et al.* [2014]; Panel c after *Mumladze et al.* [2015].

Figure 3:

Field photographs showing units and structural relations at locations indicated in Figure S1. (a) Foliated Variscan basement gneiss intruded by foliation-parallel mafic dikes of inferred Middle Jurassic age in the hanging wall of the Main Caucasus Thrust. Unit ages from *Gabkina and Ermakov* [1989]. (b) Flyschoid sedimentary rocks south of the Main Caucasus Thrust reported to be either Early-Middle Jurassic [*Kandelaki and Kakhazdze*, 1957] or Early Cretaceous (Hauterivian) [*Gudjabidze*, 2003] in age. (c) Volcaniclastic conglomerate and breccia of Late Jurassic (Kimmeridgian) age [*Melnikov and Popova*, 1975] in the southwestern part of the Greater Caucasus thrust belt. (d) Pillow basalts of Early to Middle Jurassic age [*Melnikov and Popova*, 1975] within the thrust belt. (e) Well-bedded, coarse-grained siliciclastic deposits of Late Cretaceous to Eocene age [*Kandelaki and Kakhazdze*, 1957] hosting olistostromes containing blocks of probable Cretaceous-aged carbonate.

Figure 4:

Preliminary line-length balanced regional cross section across the western Greater Caucasus at ~42°E at location shown in Figure 2a. Section was constructed from the surface geology as reported on 1:200,000-scale Soviet geologic map sheets K38-XIII [*Dzhandidze and Kandelaki*, 1957], K38-VIII [*Melnikov and Popova*, 1975], K38-VII [*Gamkrelidze and Kakhazdze*, 1959], K38-II [*Kizevalter*, 1959], K38-I [*Potapenko*, 1964], K37-XVIII [*Kandelaki*, 1957], and K37-XII [*Zdilashavili*, 1957]. Moho depth from Zor [2008]. Total shortening of ~130 km is determined by line-length balancing the basement-cover contact between the pink and purple units. The retro-deformable nature of this cross section makes it a step forward in quantifying shortening estimates in the Greater Caucasus over previous sections [e.g., *Dotduyev*, 1986]. However, ongoing geologic mapping in the vicinity of the surface trace of this cross section indicates that future refinement of this shortening estimate is expected [e.g., *Trexler et al.*, 2015].

Figure 5:

Detrital zircon U-Pb ages from the Caucasus region and an analysis of their provenance implications. Bold sample names indicate results from the present study, those in gray are published analyses of 5 Oligo-Pliocene sandstones [*Vincent et al.*, 2013], modern sediment from the Dnieper, Don, and Volga rivers [*Wang et al.*, 2011], and 1 Jurassic (Bajocian) sandstone [*Allen et al.*, 2006]. See Figures 1a and 2a for sample locations. Note separation of samples into distinct northern (Variscan and East European Craton)

and southern (Lesser Caucasus and Achara-Trialet) provenance domains. All southern samples show minimal evidence of contribution from the northern source (i.e., SE-GC, SW-GC and Tovuz River), except for Miocene sandstone samples (WG95/1 and WG66c/2), which are inferred here to have been deposited out in the Greater Caucasus Basin after it started to close. Modern sediments from rivers draining the Greater Caucasus (Inguri, Kumuk, Kura) reflect mixing of northern and southern sources, indicating their catchments span both domains. Modern sediments from Russian rivers draining the East European Craton show provenance patterns that are largely distinct from the Caucasus samples, as noted previously [*Allen et al.*, 2006; *Vincent et al.*, 2013]. (a) Age spectra shown as PDP and KDE curves [*Vermeesch*, 2012]; see panel b for legend. Samples are grouped and colored according to source areas determined in panel D from analysis of likeness (L) values [*Satkoski et al.*, 2013]. Red boxes indicate reported depositional ages, vertical colored bars indicate age spans inferred to be diagnostic of particular source areas, with blue and green bars denoting the northern (Variscan) and southern (Lesser Caucasus) source areas, respectively. (b) Legend explaining symbols used on panel a. (c) Plot showing maximum possible likeness value (L) as a function of sample size *n* (number of U-Pb ages in the detrital zircon sample), determined by sampling with replacement from a 4000-grain detrital zircon age dataset [*Pullen et al.*, 2014]. Note that L increases with increasing *n*, but rate of increase decreases with $n >$ 300. (d) Correlation matrix of normalized likeness values (L) for all samples. Four groups

of samples can be defined on the basis of the L-value correlation: East European Craton, Variscan, Mixed (East European Craton + Variscan), and Lesser Caucasus (see text for discussion).

Figure 6:

Sample locations with respect to detrital zircon provenance domains and inferred buried suture zone (geometry approximate). The location of the suture is too poorly known to show it as a discrete line, although current data indicate it is buried somewhere within the indicated zone. Additional field investigation is required to refine the location and surficial expression of the buried suture, and determine how the basin geometry evolved over time. Colors for Variscan, Lesser Caucasus, and Achara-Trialet provenance domains correspond to those used in Figure 2a. Regions concealed by younger synorogenic and Plio-Quaternary sediments shown in light gray. Diamonds and stars indicate detrital zircon samples of bedrock sandstone and modern river sediment, respectively; black lines with white edges delineate catchments above modern river samples. White dots indicate previously reported detrital zircon analyses of Oligo-Miocene [*Vincent et al.*, 2013] and Jurassic (Bajocian) [*Allen et al.*, 2006] sandstone. Gray dots show locations of other published provenance data discussed in text, including 3 samples at the Chanis River section (WG28b/3, WG28c/5, WG28c/1, and WG27/4) [*Vincent et al.*, 2014; *Vincent et al.*, 2013; *Vincent et al.*, 2007]. Schematic cross sections indicate that basin was wide during latest Cretaceous to Paleocene time, but narrow both during Jurassic opening and

late Miocene closure (ATA: Anatolide-Tauride-Armenian block; B-P: Bitlis-Pötürge; EAAC: East Anatolian Accretionary Complex).

Figure 7:

Map of Eocene magmatic rocks in Asia Minor showing a salient in the Lesser Caucasus and Talysh relative to the Pontides and Alborz to the west and east, respectively. Thick green dotted line indicates a rough estimate of the current (deformed) geometry, which appears to be deflected to the northeast by as much as 300 km relative to an assumed original geometry (thin green dotted line), prior to closure of the Greater Caucasus Basin [modified from *Allen and Armstrong*, 2008]. Heavy black line shows position of Bitlis-Zagros suture at present only. During Eocene this suture was well south of the position shown here at a location not restored in the figure. Because only Eocene rocks are shown, any bending that occurred to produce the pattern shown here must postdate any earlier phases of oroclinal bending implied by paleomagnetic data [e.g., *Meijers et al.*, 2016 in press]. The significance of the apparent eastward decrease in deflection magnitude in the Talysh is unclear. The original geometry of the belt is not well known and it may be that the thin green dotted line should be farther south at ~48°E. Alternatively, the Greater Caucasus basin may have narrowed eastwards. The reconstruction here is not precluded by Eocene magmatic rocks south of the dotted line that are due to other Neotethyan arcs/basins south of the Lesser Caucasus-Talysh system.

Figure 8:

Mesozoic-present tectonic evolution of the central Arabia-Eurasia collision zone shown schematically in map (top) and cross-section (bottom) views (T's on late Miocene map indicate approximate location of section). *Middle Jurassic*: backarc rifting of the Pontide-Lesser Caucasus arc opens the Black Sea, Caucasus, and South Caspian basins. Light gray color represents extended continental crust and/or transitional oceanic crust. *Paleocene*: The IAESA (Sevan) suture had either already closed in the latest Cretaceous (~73-71 Ma) [*Rolland et al.*, 2009; *Rolland et al.*, 2012] or did so in Paleocene time [*Sosson et al.*, 2010] via collision of the Lesser Caucasus arc and Anatolide-Tauride-Armenian. *Eocene-Oligocene*: closure of the Bitlis suture results in soft collision between Arabia and the Bitlis-Pötürge massif, causing the locus of convergence to jump northward, initiating subduction of the Caucasus relict back-arc basin. *Oligo-Miocene*: Ab-Eu plate convergence accommodated by subduction of the Greater Caucasus Basin beneath the Greater Caucasus and growth of East Anatolian Accretionary Complex, with minimal reduction in plate convergence rate. *Mio-Pliocene*: collision of the Lesser Caucasus arc with the Eurasian basement to the north at ~5 Ma leads to hard collision and accelerated uplift/exhumation of the Greater Caucasus Mountains. Geometries of ridges (paired lines) and transforms (single lines) in backarc basin are completely conjectural (black = active rifting, grey = relict). Black Sea geometry simplified by omission of Shatsky Ridge. Arrowed semi-circles indicate inferred vertical-axis rotation and oroclinal

bending of Pontide-Lesser Caucasus Arc. Barbed lines indicate subduction (solid) or sutures (hollow), barbs on upper plate. ATA: Anatolide-Tauride-Armenian block; B-P: Bitlis-Pötürge; BKF: Borjomi-Kazbegi fault; EAAC: East Anatolian Accretionary Complex; EAF: East Anatolian fault; GC: Greater Caucasus; LC: Lesser Caucasus; MRF: Main Recent Fault; NAF: North Anatolian fault; WCF: West Caspian fault. Adapted from *Zonenshain and Le Pichon* [1986], *Şengör et al.* [2003], *Sosson et al.* [2010], *Rolland et al.* [2012], *Allen et al.* [2003], *Allen and Armstrong* [2008], and *Stampfli and Borel* [2002].

Figure 9:

Both deficits and balances of upper crustal shortening should be expected within collisional orogens. Diagrams show the distribution of plate convergence into end-member components of (a) subduction without accretion, which produces no crustal shortening, (b) subduction with full accretion, in which convergence is fully recorded by crustal shortening, and (c) pure shear shortening of the orogen, which shortens the crust but does not contribute to subduction. The center panel (d) shows the most general case, where all three mechanisms operate simultaneously. In this general case, it is possible for plate convergence to either be equal to or exceed crustal shortening. Likewise, crustal shortening can be less than, equal to, or greater than the length of slab subducted since collision.

References

Abdulleyev, R. N., and R. A. Samedova (1976), Geology and petrology of magmatic formations of the Vandam zone of the Southeastern Caucasus, in *Essays on Geological Petrology*, edited by O. A. Bogatikov, A. M. Borusk and A. K. Simon, pp. 137-145, Akademia Nauka.

Adamia, S., M. B. Lordkipandize, and G. S. Zakariadze (1977), Evolution of an active continental margin as exemplified by the alpine history of the Caucasus, *Tectonophysics*, *40*, 183-199.

Adamia, S., I. P. Gamkrelidze, G. S. Zakariadze, and M. B. Lordkipandize (1974), Adzhar-Trialet trough and the problem of the Black Sea deep water trough, *Geotectonics*, *1*, 39-47.

Adamia, S., V. Alania, A. Chabukiani, Z. Kutelia, and N. Sadradze (2011), Great Caucasus (Cavcasioni): A long-lived north-Tethyan back-arc basin, *Turkish Journal of Earth Sciences*, *20*, 611-628.

Agabekov, M. G., and A. B. Moshashvili (1978), Kyurdamir-Saatly buried uplift of the Kura basin, an integral part of the Lesser Caucasus geosyncline in Cretaceous time, *Doklady of the National Academy of Sciences of the USSR*, *232*, 120-122.

Agard, P., J. Omrani, L. Jolivet, and F. Mouthereau (2005), Convergence history across Zagros (Iran): constraints from collisional and earlier deformation, *Int J Earth Sci (Geol Rundsch)*, *94*(3), 401-419.

Aitchison, J. C., J. R. Ali, and A. M. Davis (2007), When and where did India and Asia collide?, *Journal of Geophysical Research: Solid Earth*, *112*(B5), B05423.

Aldanmaz, E., J. A. Pearce, M. F. Thirlwall, and J. G. Mitchell (2000), Petrogenetic evolution of late Cenozoic, post-collision volcanism in western Anatolia, Turkey, *Journal of Volcanology and Geothermal Research*, *102*(1–2), 67-95.

Ali, J. R., and J. C. Aitchison (2006), Positioning Paleogene Eurasia problem: Solution for 60–50 Ma and broader tectonic implications, *Earth and Planetary Science Letters*, *251*(1–2), 148-155.

Ali, S. A., S. Buckman, K. J. Aswad, B. G. Jones, S. A. Ismail, and A. P. Nutman (2013), The tectonic evolution of a Neo-Tethyan (Eocene–Oligocene) island-arc (Walash and Naopurdan groups) in the Kurdistan region of the Northeast Iraqi Zagros Suture Zone, *Island Arc*, *22*(1), 104-125.

Ali-Zade, A. A., et al. (2005), Geological Map of Azerbaijan Republic, Geology Institute National Academy of Sciences of Azerbaijan Republic.

Allen, M. B., and H. A. Armstrong (2008), Arabia–Eurasia collision and the forcing of mid-Cenozoic global cooling, *Palaeogeography, Palaeoclimatology, Palaeoecology*, *265*(1–2), 52-58.

Allen, M. B., J. Jackson, and R. Walker (2004), Late Cenozoic reorganization of the Arabia-Eurasia collision and the comparison of short-term and long-term deformation rates, *Tectonics*, *23*.
Allen, M. B., S. Jones, A. Ismail-Zadeh, M. Simmons, and L. Anderson (2002), Onset of subduction as the cause of rapid Pliocene-Quaternary subsidence in the South Caspian basin, *Geology*, *30*(9), 775-778.
Allen, M. B., S. J. Vincent, G. I. Alsop, A. Ismail-Zadeh, and R. Flecker (2003), Late Cenozoic deformation in the South Caspian region: effects of a rigid basement block within a collision zone, *Tectonophysics*, *366*, 223-239.
Allen, M. B., A. C. Morton, C. M. Fanning, A. Ismail-Zadeh, and S. B. Kroonenberg (2006), Zircon age constraints on sediment provenance in the Caspian region, *Journal of the Geological Society of London*, *163*, 647-655.
Allmendinger, R. W., and T. Gubbels (1996), Pure and simple shear plateau uplift, Altiplano-Puna, Argentina and Bolivia, *Tectonophysics*, *259*, 1-13.
Andersen, T. (2005), Detrital zircons as tracers of sedimentary provenance: limiting conditions from statistics and numerical simulation, *Chemical Geology*, *216*(3–4), 249-270.
Argus, D. F., R. G. Gordon, M. B. Heflin, C. Ma, R. J. Eanes, P. Willis, W. R. Peltier, and S. E. Owen (2010), The angular velocities of the plates and the velocity of Earth's centre from space geodesy, *Geophysical Journal International*, *180*(3), 913-960.
Austermann, J., and G. Iaffaldano (2013), The role of the Zagros orogeny in slowing down Arabia-Eurasia convergence since ~5 Ma, *Tectonics*, *32*(3), 351-363.
Avagyan, A., M. Sosson, A. Karakhanian, H. Philip, S. Rebai, Y. Rolland, R. Melkonyan, and V. Davtyan (2010), Recent tectonic stress evolution in the Lesser Caucasus and adjacent regions, *Geological Society, London, Special Publications*, *340*(1), 393-408.
Avdeev, B. (2011), Tectonics of the Greater Caucasus and the Arabia-Eurasia Orogen, 137 pp, University of Michigan, Ann Arbor.
Avdeev, B., and N. A. Niemi (2011), Rapid Pliocene exhumation of the central Greater Caucasus constrained by low-temperature thermochronometry, *Tectonics*, *30*.
Axen, G. J., P. S. Lam, M. Grove, D. F. Stockli, and J. Hassanzadeh (2001), Exhumation of the west-central Alborz Mountains, Iran, Caspian subsidence, and collision-related tectonics, *Geology*, *29*(6), 559-562.
Azizbekov, S. A., and G. S. Dzotsenidze (1971), Magmatism in the Caucasus, Iran and Turkey, *International Geology Review*, *13*(10), 1464-1470.
Ballato, P., C. E. Uba, A. Landgraf, M. R. Strecker, M. Sudo, D. F. Stockli, A. Friedrich, and S. H. Tabatabaei (2011), Arabia-Eurasia continental collision: Insights from late Tertiary foreland-basin evolution in the Alborz Mountains, northern Iran, *Geological Society of America Bulletin*, *123*(1-2), 106-131.

Ballato, P., D. F. Stockli, M. R. Ghassemi, A. Landgraf, M. R. Strecker, J. Hassanzadeh, A. Friedrich, and S. H. Tabatabaei (2013), Accommodation of transpressional strain in the Arabia-Eurasia collision zone: new constraints from (U-Th)/He thermochronology in the Alborz mountains, north Iran, *Tectonics*, *32*(1), 1-18.

Ballato, P., A. Landgraf, T. F. Schildgen, D. F. Stockli, M. Fox, M. R. Ghassemi, E. Kirby, and M. R. Strecker (2015), The growth of a mountain belt forced by base-level fall: Tectonics and surface processes during the evolution of the Alborz Mountains, N Iran, *Earth and Planetary Science Letters*, *425*, 204-218.

Banks, C. J., A. G. Robinson, and M. P. Williams (1997), Structure and regional tectonics of the Achara-Trialet fold belt and the adjacent Rioni and Karli foreland basins, Republic of Georgia, in *Regional and petroleum geology of the Black Sea and surrounding region*, edited by A. G. Robinson, pp. 331-346.

Bazhenov, M. L., and V. S. Burtman (1989), Paleomagentism of Upper Cretaceous Rocks from the Caucasus and Its Implications for Tectonics, in *Tectonic Evolution of the Tethyan Region*, edited by A. M. C. Sengor, pp. 217-239, Kluwer Academic Publishing.

Bazhenov, M. L., and V. S. Burtman (2002), Eocene paleomagnetism of the Caucasus (southwest Georgia): oroclinal bending in the Arabian syntaxis, *Tectonophysics*, *344*, 247-259.

Belov, A. A., M. L. Somin, and S. A. Adamiya (1978), Precambrian and Paleozoic of the Caucasus (brief synthesis), *Jahrbuch der Geologischen B.-A*, *121*(1), 155-175.

Berberian, M. (1995), Master "blind" thrust faults hidden under the Zagros folds: active basement tectonics and surface morphotectonics, *Tectonophysics*, *241*, 193-224.

Bogdanova, S. V., B. Bingen, R. Gorbatschev, T. N. Kheraskova, V. I. Kozlov, V. N. Puchkov, and Y. A. Volozh (2008), The East European Craton (Baltica) before and during the assembly of Rodinia, *Precambrian Research*, *160*(1–2), 23-45.

Botev, Z. I., J. F. Grotowski, and D. P. Kroese (2010), Kernel density estimation via diffusion, *Annals of Statistics*, *38*, 2816-2957.

Bouilhol, P., O. Jagoutz, J. M. Hanchar, and F. O. Dudas (2013), Dating the India–Eurasia collision through arc magmatic records, *Earth and Planetary Science Letters*, *366*(0), 163-175.

Boulton, S. J., and A. H. F. Robertson (2007), The Miocene of the Hatay area, S Turkey: Transition from the Arabian passive margin to an underfilled foreland basin related to closure of the Southern Neotethys Ocean, *Sedimentary Geology*, *198*(1–2), 93-124.

Brandon, M. T. (1996), Probability density plot for fission-track grain-age samples, *Radiation Measurements*, *26*(5), 663-676.

Brunet, M.-F., M. V. Korotaev, A. V. Ershov, and A. M. Nikishin (2003), The South Caspian Basin: a review of its evolution from subsidence modelling, *Sedimentary Geology*, *156*, 119-148.

Capitanio, F. A., and A. Replumaz (2013), Subduction and slab breakoff controls on Asian indentation tectonics and Himalayan western syntaxis formation, *Geochemistry, Geophysics, Geosystems, 14*(9), 3515-3531.
Capitanio, F. A., G. Morra, S. Goes, R. F. Weinberg, and L. Moresi (2010), India-Asia convergence driven by the subduction of the Greater Indian continent, *Nature Geoscience*, *3*(2), 136-139.
Carroll, A. R., Y. Liang, S. A. Graham, X. Xiao, M. S. Hendrix, J. Chu, and C. L. McKnight (1990), Junggar basin, northwest China: trapped Late Paleozoic ocean, *Tectonophysics*, *181*, 1-14.
Catalán, J. R. M., J. FernÁndez-SuÁrez, G. A. Jenner, E. Belousova, and A. Montes (2004), Provenance constraints from detrital zircon U–Pb ages in the NW Iberian Massif: implications for Palaeozoic plate configuration and Variscan evolution, *J. Geol. Soc.*, *161*(3), 463-476.
Clark, M. K. (2012), Continental collision slowing due to viscous mantle lithosphere rather than topography, *Nature*, *483*(7387), 74-77.
Copley, A., J.-P. Avouac, and J.-Y. Royer (2010), India-Asia collision and the Cenozoic slowdown of the Indian plate: Implications for the forces driving plate motions, *Journal of Geophysical Research: Solid Earth*, *115*(B3), B03410.
Cowgill, E. (2010), Cenozoic right-slip faulting along the eastern margin of the Pamir salient, northwestern China, *Geological Society of America Bulletin*, *122*(1/2), 145-161.
DeCelles, P. G., and K. A. Giles (1996), Foreland basin systems, *Basin Research, 8*, 105-123.
Dewey, J. F. (1977), Suture zone complexities; a review, *Tectonophysics*, *40*, 53-67.
Dewey, J. F., and K. Burke (1974), Hot Spots and Continental Break-up: Implications for Collisional Orogeny, *Geology*, *2*(2), 57-60.
Dewey, J. F., S. Cande, and W. C. Pitman (1989), Tectonic evolution of the India/Eurasia collision zone, *Eclogae Geologicae Helvetiae*, *82*(3), 717-734.
Dickinson, W. R., and G. E. Gehrels (2003), U–Pb ages of detrital zircons from Permian and Jurassic eolian sandstones of the Colorado Plateau, USA: paleogeographic implications, *Sedimentary Geology*, *163*(1–2), 29-66.
Dotduyev, S. I. (1986), Nappe structure of the Greater Caucasus range, *Geotectonics*, *20*(5), 420-430.
Dzhanelidze, A. I., and N. A. Kandelaki (1957), K-38-XIII, Ministry of Geology and Mineral Protection USSR, Moscow.
Elmore, R. D., O. H. Pilkey, W. J. Cleary, and H. A. Curran (1979), Black Shell turbidite, Hatteras Abyssal Plain, western Atlantic Ocean, *Geological Society of America Bulletin*, *90*(12), 1165-1176.

Ershov, A. V., M.-F. Brunet, A. M. Nikishin, S. N. Bolotov, B. P. Nazarevich, and M. V. Korotaev (2003), Northern Caucasus basin: thermal history and synthesis of subsidence models, *Sedimentary Geology*, *156*, 95-118.

Fedo, C. M., K. N. Sircombe, and R. H. Rainbird (2003), Detrital Zircon Analysis of the Sedimentary Record, *Reviews in Mineralogy and Geochemistry*, *53*(1), 277-303.

Flesch, L. M., A. J. Haines, and W. E. Holt (2001), Dynamics of the India-Eurasia collision zone, *Journal of Geophysical Research*, *106*(B8), 16435-16460.

Forte, A. M. (2012), Late Cenozoic Evolution of the Greater Caucasus Mountains and Kura Foreland Basin: Implications for Early Orogenesis, University of California, Davis.

Forte, A. M., E. Cowgill, and K. X. Whipple (2014), Transition from a singly vergent to doubly vergent wedge in a young orogen: The Greater Caucasus, *Tectonics*, *33*(11), 2014TC003651.

Forte, A. M., K. X. Whipple, B. Bookhagen, and M. W. Rossi (2016), Decoupling of modern shortening rates, climate, and topography in the Caucasus, *Earth and Planetary Science Letters*, *449*, 282-294.

Forte, A. M., E. Cowgill, T. Bernardin, O. Kreylos, and B. Hamann (2010), Late Cenozoic deformation of the Kura fold-thrust belt, southern Greater Caucasus, *Geological Society of America Bulletin*, *122*(3/4), 465-486.

Forte, A. M., E. Cowgill, I. Murtuzayev, T. Kangarli, and M. Stoica (2013), Structural geometries and magnitude of shortening in the eastern Kura fold-thrust belt, Azerbaijan: Implications for the development of the Greater Caucasus Mountains, *Tectonics*, *32*(3), 688-717.

Forte, A. M., D. Y. Sumner, E. Cowgill, M. Stoica, I. Murtuzayev, T. Kangarli, M. Elashvili, T. Godoladze, and Z. Javakhishvili (2015), Late Miocene to Pliocene stratigraphy of the Kura Basin, a subbasin of the South Caspian Basin: Implications for the diachroneity of stage boundaries, *Basin Research*, *27*(3), 247-271.

Gamkrelidze, I. P. (1986), Geodynamic evolution of the Caucasus and adjacent areas in Alpine time, *Tectonophysics*, *127*, 261-277.

Gamkrelidze, I. P., and D. M. Shengelia (2001), Origin of the igneous rocks of the Dzirula crystalline massif (Caucasus) in light of the tectonic layering of the Earths' crust, *Geotectonics*, *35*(1), 51-61.

Gamkrelidze, I. P., G. D. Dumbadze, M. A. Kekeliya, I. I. Khmaladze, and O. D. Khutsishvili (1981), Ophiolites of the Dzirul Massif and the Caucasus, *Geotectonics*, *15*(5), 389-396.

Gamkrelidze, P. D., and I. R. Kakhazdze (1959), K-38-VII, Ministry of Geology and Mineral Protection USSR, Moscow.

Gehrels, G. (2012), Detrital Zircon U-Pb Geochronology: Current Methods and New Opportunities, in *Tectonics of Sedimentary Basins: Recent Advances*, edited by C. Busby and A. A. Pérez, pp. 47-62, Blackwell Publishing Ltd.

Gehrels, G. (2014), Detrital Zircon U-Pb Geochronology Applied to Tectonics, *Annual Review of Earth and Planetary Sciences*, *42*(1), 127-149.

Gehrels, G., V. Valencia, and A. Pullen (2006), Detrital zircon geochronology by laser-ablation multicollector ICPMS at the Arizona LaserChron Center, in *Geochronology: Emerging Opportunities, Paleontological Society Short Course, October 21, 2006*, edited by T. Olszewski, Paleontological Society Papers, Philadelphia, PA.

Gehrels, G. E., and W. R. Dickinson (1995), Detrital zircon provenance of Cambrian to Triassic miogeoclinal and eugeoclinal strata in Nevada, *American Journal of Science*, *295*(1), 18-48.

Gehrels, G. E., V. A. Valencia, and J. Ruiz (2008), Enhanced precision, accuracy, efficiency, and spatial resolution of U-Pb ages by laser ablation–multicollector–inductively coupled plasma–mass spectrometry, *Geochemistry, Geophysics, Geosystems*, *9*(3), Q03017.

Golonka, J. (2007), Geodynamic evolution of the South Caspian Basin, in *Oil and gas of the Greater Caspian Area*, edited by P. O. Yilmaz and G. H. Isaken, pp. 17-41.

Graham, S. A., W. R. Dickinson, and R. V. Ingersoll (1975), Himalayan-Bengal Model for Flysch Dispersal in the Appalachian-Ouachita System, *Geological Society of America Bulletin*, *86*(3), 273-286.

Gubkina, A. N., and V. A. Ermakov (1989), K-38-IX, USSR Ministry of Geology, Leningrad.

Gudjabidze, G. E. (2003), Geological Map of Georgia, Georgian State Department of Geology and National Oil Company "SAQNAVTOBI".

Guest, B., G. J. Axen, P. S. Lam, and J. Hassanzadeh (2006), Late Cenozoic shortening in the west-central Alborz Mountains, northern Iran, by combined conjugate strike-slip and thin-skinned deformation, *Geosphere*, *2*(1), 35-52.

Guillot, S., E. Garzanti, D. Baratoux, D. Marquer, G. Mahéo, and J. de Sigoyer (2003), Reconstructing the total shortening history of the NW Himalaya, *Geochemistry, Geophysics, Geosystems*, *4*(7), 1064.

Hanel, M., A. G. Gurbanov, and H. J. Lippolt (1992), Age and genesis of granitoids from the Main-Range and Bechasyn Zones of the western Greater Caucasus, *Neues Jahrbuch fur Mineralogie Monatshefte*, *12*, 529-544.

Hassanzadeh, J., D. F. Stockli, B. K. Horton, G. J. Axen, L. D. Stockli, M. Grove, A. K. Schmitt, and J. D. Walker (2008), U-Pb zircon geochronology of late Neoproterozoic–Early Cambrian granitoids in Iran: Implications for paleogeography, magmatism, and exhumation history of Iranian basement, *Tectonophysics*, *451*(1–4), 71-96.

Hatzfeld, D., and P. Molnar (2010), Comparisons of the kinematics and deep structures of the Zagros and Himalaya and of the Iranian and Tibetan plateaus and geodynamic implications, *Rev. Geophys.*, *48*(2), RG2005.

Haug, G. H., and R. Tiedemann (1998), Effect of the formation of the Isthmus of Panama on Atlantic Ocean thermohaline circulation, *Nature*, *393*(6686), 673-676.

Hempton, M. R. (1985), Structure and deformation history of the Bitlis suture near Lake Hazar, southeastern Turkey, *Geological Society of America Bulletin*, *96*(2), 233-243.

Hempton, M. R. (1987), Constraints on Arabian Plate motion and extensional history of the Red Sea, *Tectonics*, *6*(6), 687-705.

Hsü, K. J. (1988), Relict back-arc basins: Principles of recognition and possible new examples from China, in *New Perspectives in Basin Analysis*, edited by K. L. Kleinsphen and C. Paola, pp. 245-263, Springer-Verlag, New York, NY.

Ingersoll, R. V. (2012), Tectonics of sedimentary basins, with revised nomenclature, in *Tectonics of Sedimentary Basins: Recent Advances*, edited by C. Busby and A. A. Pérez, pp. 3-43, Blackwell Publishing Ltd.

Ingersoll, R. V., and C. J. Busby (1995), Tectonics of sedimentary basins, in *Tectonics of Sedimentary Basins*, edited by C. J. Busby and R. V. Ingersoll, pp. 1-51, Blackwell Scientific, Cambridge, MA.

Ingersoll, R. V., S. A. Graham, and W. R. Dickinson (1995), Remnant ocean basins, in *Tectonics of Sedimentary Basins*, edited by C. J. Busby and R. V. Ingersoll, pp. 363-391, Blackwell Scientific, Cambridge, MA.

Jackson, J. (1992), Partitioning of strike-slip and convergent motion between Eurasia and Arabia in eastern Turkey and the Caucasus, *Journal of Geophysical Research*, *97*(B9), 12,471-412,479.

Jackson, J., K. Priestley, M. B. Allen, and M. Berberian (2002), Active tectonics of the South Caspian Basin, *Geophysical Journal International*, *148*(2), 214-245.

Kandelaki, D. N., and I. R. Kakhazdze (1957), K-38-XV, Ministry of Geology and Mineral Protection USSR, Moscow.

Kandelaki, N. A. (1957), K-37-XVIII, Ministry of Geology and Mineral Protection USSR, Moscow.

Karig, D. E. (1971), Origin and development of marginal basins in the western Pacific, *Journal of Geophysical Research*, *76*(11), 2542-2561.

Kazmin, V. G., A. A. Schreider, and A. A. Bulychev (2000), Early stages of evolution of the Black Sea, in *Tectonics and Magmatism in Turkey and the Surrounding Area*, edited by E. Bozkurt, J. A. Winchester and J. D. A. Piper, pp. 235-249, Geological Society, London.

Kazmin, V. G., I. M. Sbortshikov, L. E. Ricou, L. P. Zonenshain, J. Boulin, and A. L. Knipper (1986), Volcanic belts as markers of the Mesozoic-Cenozoic active margin of Eurasia, *Tectonophysics*, *123*(1–4), 123-152.

Kelty, T. K., A. Yin, B. Dash, G. E. Gehrels, and A. E. Ribeiro (2008), Detrital-zircon geochronology of Paleozoic sedimentary rocks in the Hangay–Hentey basin, north-central Mongolia: Implications for the tectonic evolution of the Mongol–Okhotsk Ocean in central Asia, *Tectonophysics*, *451*(1–4), 290-311.

Keskin, M. (2003), Magma generation by slab steepening and breakoff beneath a subduction-accretion complex: An alternative model for collision-related volcanism in Eastern Anatolia, Turkey, *Geophysical Research Letters*, *30*(24).

Keskin, M., J. A. Pearce, and J. G. Mitchell (1998), Volcano-stratigraphy and geochemistry of collision-related volcanism on the Erzurum-Kars Plateau, North Eastern Turkey, *Journal of Volcanology and Geothermal Research*, *85*(1-4), 355-404.

Khain, V. E. (2007), Mesozoic-Cenozoic accretionary complexes of the Greater Caucasus, *Dokl. Earth Sc.*, *413*(2), 376-379.

Khain, V. E., and A. N. Shardanov (1960), K-39-XXV, Ministry of Geology and Mineral Protection USSR, Moscow.

Khain, V. E., and L. I. Lobkovskiy (1994), Relict seismicity in the Alpine belt of Eurasia: Mode of occurence, *Geotectonics*, *28*(3), 192-198.

Khalilov, E. N., S. F. Mekhtiyev, and Y. Khain (1987), Some geophysical data confirming the collisional origin of the Greater Caucasus, *Geotectonics*, *21*(2), 132-136.

Kizevalter, D. S. (1959), K-38-II, Ministry of Geology and Mineral Protection USSR, Moscow.

Knapp, C. C., J. H. Knapp, and J. A. Connor (2004), Crustal-scale structure of the South Caspian Basin revealed by deep seismic reflection profiling, *Marine and Petroleum Geology*, *21*(8), 1073-1081.

Kocyigit, A., A. Yilmaz, S. Adamia, and S. Kuloshvili (2001), Neotectonics of East Anatolia Plateau (Turkey) and Lesser Caucasus: implication for transition from thrusting to strike-slip faulting, *Geodinamica Acta*, *14*, 177-195.

Kopp, M. L. (1985), Age and nature of deformations of sediments comprising the Lagich Syncline, *Moscow University Geology Bulletin*, *40*(1), 23-32.

Kopp, M. L., and I. G. Shcherba (1985), Late alpine development of the east Caucasus, *Geotectonics*, *19*(6), 497-507.

Kral, J., and A. G. Gurbanov (1996), Apatite fission track data from the Great Caucasus pre-Alpine basement, *Chemie der Erde*, *56*(2), 177-192.

Li, G., and A. J. West (2014), Evolution of Cenozoic seawater lithium isotopes: Coupling of global denudation regime and shifting seawater sinks, *Earth and Planetary Science Letters*, *401*, 284-293.

Lippert, P. C., D. J. J. van Hinsbergen, and G. Dupont-Nivet (2014), Early Cretaceous to present latitude of the central proto-Tibetan Plateau: A paleomagnetic synthesis

with implications for Cenozoic tectonics, paleogeography, and climate of Asia, *Geological Society of America Special Papers*, *507*, 1-21.
Mangino, S., and K. Priestley (1998), The crustal structure of the southern Caspian region, *Geophysical Journal International*, *133*, 630-648.
Markus, M. A., and A. M. Miroshanikov (2001), K-38-XVII, Ministry of Natural Resources of the Russian Federation, Moscow.
Mayringer, F., P. J. Treloar, A. Gerdes, F. Finger, and D. Shengelia (2011), New age data from the Dzirula massif, Georgia: Implications for the evolution of the Caucasian Variscides, *American Journal of Science*, *311*(5), 404-441.
McClusky, S., et al. (2000), Global positioning system constraints on plate kinematics and dynamics in the eastern Mediterranean and Caucasus, *Journal of Geophysical Research*, *105*(B3), 5695-5719.
McKenzie, D. (1972), Active Tectonics of the Mediterranean Region, *Geophysical Journal of the Royal Astronomical Society*, *30*(2), 109-185.
McQuarrie, N., and D. J. J. van Hinsbergen (2013), Retrodeforming the Arabia-Eurasia collision zone: Age of collision versus magnitude of continental subduction, *Geology*, *41*(3), 315-318.
McQuarrie, N., J. M. Stock, C. Verdel, and B. P. Wernicke (2003), Cenozoic evolution of Neotethys and implications for the causes of plate motions, *Geophysical Research Letters*, *30*(20).
Mederer, J., R. Moritz, A. Ulianov, and M. Chiaradia (2013), Middle Jurassic to Cenozoic evolution of arc magmatism during Neotethys subduction and arc-continent collision in the Kapan Zone, southern Armenia, *Lithos*, *177*(0), 61-78.
Meijers, M. J. M., et al. (2015), A paleolatitude reconstruction of the South Armenian Block (Lesser Caucasus) for the Late Cretaceous: Constraints on the Tethyan realm, *Tectonophysics*, *644–645*(0), 197-219.
Meijers, M. J. M., et al. (2016 in press), Progressive orocline formation in the Eastern Pontides–Lesser Caucasus, in *Tectonic Evolution of the Eastern Black Sea and Caucasus*, edited by M. Sosson, R. A. Stephenson and S. A. Adamia, Geological Society, London, Special Publications, 428, doi: 10.1144/SP428.8.
Mellors, R. J., J. Jackson, S. Myers, R. Gok, K. Priestley, G. Yetirmishli, N. Turkelli, and T. Godoladze (2012), Deep Earthquakes beneath the Northern Caucasus: Evidence of Active or Recent Subduction in Western Asia, *Bulletin of the Seismological Society of America*, *102*(2), 862-866.
Melnikov, V. A., and E. I. Popova (1975), K-38-VIII, USSR Ministry of Geology, Moscow.
Molnar, P., and H. Lyon-Caen (1988), Some simple physical aspects of the support, structure, and evolution of mountain belts, in *Processes in Continental Lithospheric Deformation*, edited by S. P. Clark, B. C. Burchfiel and J. Suppe, pp. 179-207, Geological Society of America Special Paper 218, Boulder.

Molnar, P., and J. M. Stock (2009), Slowing of India's convergence with Eurasia since 20 Ma and its implications for Tibetan mantle dynamics, *Tectonics*, *28*(3), TC3001.
Molnar, P., D. Freedman, and J. S. F. Shih (1979), Lengths of intermediate and deep seismic zones and temperatures in downgoing slabs of lithosphere, *Geophysical Journal of the Royal Astronomical Society*, *56*, 41-54.
Moritz, R., et al. (2016), Long-lived, stationary magmatism and pulsed porphyry systems during Tethyan subduction to post-collision evolution in the southernmost Lesser Caucasus, Armenia and Nakhitchevan, *Gondwana Research*, *37*, 465-503.
Mumladze, T., A. M. Forte, E. S. Cowgill, C. C. Trexler, N. A. Niemi, M. Burak Yıkılmaz, and L. H. Kellogg (2015), Subducted, detached, and torn slabs beneath the Greater Caucasus, *GeoResJ*, *5*(0), 36-46.
Munteanu, I., L. Matenco, C. Dinu, and S. Cloetingh (2011), Kinematics of back-arc inversion of the Western Black Sea Basin, *Tectonics*, *30*(5), TC5004.
Nalivkin, D. V. (1973), The Mediterranean Geosyncline, in *Geology of the U.S.S.R. (English Translation)*, edited by D. V. Nalivkin, pp. 578-685, Oliver and Boyd, Edinburgh.
Nalivkin, D. V. (1976), Geologic Map of the Caucasus, Ministry of Geology, USSR.
Natal'in, B. A., and A. M. C. Şengör (2005), Late Palaeozoic to Triassic evolution of the Turan and Scythian platforms: The pre-history of the Palaeo-Tethyan closure, *Tectonophysics*, *404*, 175-202.
Nikishin, A. M., A. V. Ershov, and V. A. Nikishin (2010), Geological history of Western Caucasus and adjacent foredeeps based on analysis of the regional balanced section, *Dokl. Earth Sc.*, *430*(2), 155-157.
Nikishin, A. M., P. A. Ziegler, S. N. Bolotov, and P. A. Fokin (2011), Late Paleozoic to Cenozoic evolution of the Black Sea-southern Eastern Europe region: a view from the Russian Platform, *Turkish Journal of Earth Sciences*, *20*, 571-634.
Nikishin, A. M., P. A. Ziegler, D. I. Panov, B. P. Nazarevich, M.-F. Brunet, R. A. Stephenson, S. N. Bolotov, M. V. Korotaev, and P. L. Tikhomirov (2001), Mesozoic and Cainozoic evolution of the Scythian Platform-Black Sea-Caucasus domain, in *Peri-Tethys Memoir 6: Peri-Tethyan Rift/Wrench Basins and Passive Margins, Mémoires du Muséum National D'Histoire Naturelle Tome 186*, edited by P. A. Ziegler, W. Cavazza, A. H. F. Robertson and S. Crasquin-Soleau, pp. 295-346, Publications Scientifiques Du Muséum, Paris.
Oberhänsli, R., R. Bousquet, O. Candan, and A. I. Okay (2012), Dating subduction events in East Anatolia, Turkey, *Turkish Journal of Earth Sciences*, *21*, 1-17.
Oberhänsli, R., O. Candan, R. Bousquet, G. Rimmele, A. Okay, and J. Goff (2010), Alpine high pressure evolution of the eastern Bitlis complex, SE Turkey, *Geological Society, London, Special Publications*, *340*(1), 461-483.

Okay, A. I., A. M. Celal Şengör, and N. Görür (1994), Kinematic history of the opening of the Black Sea and its effect on the surrounding regions, *Geology*, *22*(3), 267-270.
Okay, A. I., M. Zattin, and W. Cavazza (2010), Apatite fission-track data for the Miocene Arabia-Eurasia collision, *Geology*, *38*(1), 35-38.
Oldow, J. S., A. W. Bally, and H. G. Avé Lallemant (1990), Transpression, orogenic float, and lithospheric balance, *Geology*, *18*(10), 991-994.
Patriat, P., and J. Achache (1984), India-Eurasia collision chronology has implications for crustal shortening and driving mechanism of plates, *Nature*, *311*, 615-621.
Pearce, J. A., J. F. Bender, S. E. De Long, W. S. F. Kidd, P. J. Low, Y. Güner, F. Saroglu, Y. Yilmaz, S. Moorbath, and J. G. Mitchell (1990), Genesis of collision volcanism in Eastern Anatolia, Turkey, *Journal of Volcanology and Geothermal Research*, *44*(1–2), 189-229.
Perchuk, A., and P. Philippot (1997), Rapid cooling and exhumation of eclogitic rocks from the Great Caucasus, Russia, *Journal of Metamorphic Geology*, *15*(3), 299-310.
Philip, H., A. Cisternas, A. Gvishiani, and A. Gorshkov (1989), The Caucasus: an actual example of the initial stages of continental collision, *Tectonophysics*, *161*, 1-21.
Philippot, P., J. Blichert-Toft, A. Perchuk, S. Costa, and V. Gerasimov (2001), Lu–Hf and Ar–Ar chronometry supports extreme rate of subduction zone metamorphism deduced from geospeedometry, *Tectonophysics*, *342*(1–2), 23-38.
Piper, D. J. W., and A. Aksu (1987), The source and origin of the 1929 grand banks turbidity current inferred from sediment budgets, *Geo-Marine Letters*, *7*(4), 177-182.
Potapenko, Y. Y. (1964), K-38-I, Ministry of Geology and Mineral Protection USSR, Moscow.
Priestley, K., C. Baker, and J. Jackson (1994), Implications of earthquake focal mechanism data for the active tectonics of the south Caspian Basin and surrounding regions, *Geophysical Journal International*, *118*, 111-141.
Pullen, A., M. Ibanez-Mejia, G. E. Gehrels, J. C. Ibanez-Mejia, and M. Pecha (2014), What happens when n= 1000? Creating large-n geochronological datasets with LA-ICP-MS for geologic investigations, *Journal of Analytical Atomic Spectrometry*, *29*(6), 971-980.
Raymo, M. E., and W. F. Ruddiman (1992), Tectonic forcing of late Cenozoic climate, *Nature*, *359*, 117-122.
Raymo, M. E., W. F. Ruddiman, and P. N. Froelich (1988), Influence of late Cenozoic mountain building on ocean geochemical cycles, *Geology*, *16*, 649-653.
Rebaï, S., H. Philip, L. Dorbath, B. Borissoff, H. Haessler, and A. Cisternas (1993), Active tectonics in the Lesser Caucasus: coexistence of compressive and extensional structures, *Tectonics*, *12*(5), 1089-1114.

Reilinger, R., et al. (2006), GPS constraints on continental deformation in the Africa-Arabia-Eurasia continental collision zone and implications for the dynamics of plate interactions, *Journal of Geophysical Research, 111*.
Replumaz, A., S. Guillot, A. Villaseñor, and A. M. Negredo (2013), Amount of Asian lithospheric mantle subducted during the India/Asia collision, *Gondwana Research, 24*(3–4), 936-945.
Replumaz, A., F. A. Capitanio, S. Guillot, A. M. Negredo, and A. Villaseñor (2014), The coupling of Indian subduction and Asian continental tectonics, *Gondwana Research, 26*(2), 608-626.
Robinson, A. G., J. H. Rudat, C. J. Banks, and R. L. F. Wiles (1996), Petroleum geology of the Black Sea, *Marine and Petroleum Geology, 13*(2), 195-223.
Robinson, A. G., E. T. Griffith, A. R. Gardiner, and A. K. Home (1997), Petroleum geology of the Georgian fold and thrust belts and foreland basins, in *Regional and petroleum geology of the Black Sea and surrounding region*, edited by A. G. Robinson, pp. 347–367, AAPG Memoir 68.
Rolland, Y., M. Sosson, S. Adamia, and N. Sadradze (2011), Prolonged Variscan to Alpine history of an active Eurasian margin (Georgia, Armenia) revealed by 40Ar/39Ar dating, *Gondwana Research, 20*(4), 798-815.
Rolland, Y., S. Billo, M. Corsini, M. Sosson, and G. Galoyan (2009), Blueschists of the Amassia-Stepanavan Suture Zone (Armenia): linking Tethys subduction history from E-Turkey to W-Iran, *Int J Earth Sci (Geol Rundsch), 98*(3), 533-550.
Rolland, Y., D. Perincek, N. Kaymakci, M. Sosson, E. Barrier, and A. Avagyan (2012), Evidence for ~80-75 Ma subduction jump during Anatolide-Tauride-Armenian block accretion and ~48 Ma Ma Arabia-Eurasia collision in Lesser Caucasus-East Anatolia, *Journal of Geodynamics, 56-57*, 76-85.
Rolland, Y., M. Hässig, D. Bosch, M. J. M. Meijers, M. Sosson, O. Bruguier, S. Adamia, and N. Sadradze (2016), A review of the plate convergence history of the East Anatolia-Transcaucasus region during the Variscan: Insights from the Georgian basement and its connection to the Eastern Pontides, *Journal of Geodynamics, 96*, 131-145, doi 10.1016/j.jog.2016.03.003.
Ruddiman, W. F., and J. E. Kutzbach (1989), Forcing of late Cenozoic northern hemisphere climate by plateau uplift in southern Asia and the American west, *Journal of Geophysical Research: Atmospheres, 94*(D15), 18409-18427.
Safarov, I. B. (2006), Petrophysical properties of rocks in seismogenic crustal blocks of the southeastern Greater Caucasus and their geological and geophysical interpretation, *Izvestiya, Physics of the Solid Earth, 42*(3), 260-270.
Safonova, I., S. Maruyama, T. Hirata, Y. Kon, and S. Rino (2010), LA ICP MS U–Pb ages of detrital zircons from Russia largest rivers: Implications for major granitoid events in Eurasia and global episodes of supercontinent formation, *Journal of Geodynamics, 50*(3–4), 134-153.

Sahakyan, L., D. Bosch, M. Sosson, A. Avagyan, G. Galoyan, Y. Rolland, O. Bruguier, Z. Stepanyan, B. Galland, and S. Vardanyan (2016), Geochemistry of the Eocene magmatic rocks from the Lesser Caucasus area (Armenia): evidence of a subduction geodynamic environment, *Geological Society, London, Special Publications, 428*.

Satkoski, A. M., B. H. Wilkinson, J. Hietpas, and S. D. Samson (2013), Likeness among detrital zircon populations—An approach to the comparison of age frequency data in time and space, *Geological Society of America Bulletin*, *125*(11-12), 1783-1799.

Şengör, A. M. C. (1984), The Cimmeride Orogenic System and the Tectonics of Eurasia, *Geological Society of America Special Paper*, *195*, 1-82.

Şengör, A. M. C., S. Özeren, T. Genç, and E. Zor (2003), East Anatolian high plateau as a mantle-supported, north-south shortened domal structure, *Geophysical Research Letters*, *30*(24).

Şengör, A. M. C., M. S. Özeren, M. Keskin, M. Sakınç, A. D. Özbakır, and İ. Kayan (2008), Eastern Turkish high plateau as a small Turkic-type orogen: Implications for post-collisional crust-forming processes in Turkic-type orogens, *Earth-Science Reviews*, *90*(1–2), 1-48.

Shikalibeily, E. S., R. N. Abdullayev, and A. A. Ali-Zade (1988), Geological results from the Saatly superdeep drillhole, *International Geology Review*, *30*(12), 1272-1277.

Simmons, N. A., S. C. Myers, and G. Johannesson (2011), Global-scale P wave tomography optimized for prediction of teleseismic and regional travel times for Middle East events: 2. Tomographic inversion, *Journal of Geophysical Research: Solid Earth*, *116*(B4), B04305.

Skobeltsyn, G., R. Mellors, R. Gök, N. Türkelli, G. Yetirmishli, and E. Sandvol (2014), Upper mantle S wave velocity structure of the East Anatolian-Caucasus region, *Tectonics*, *33*.

Sobornov, K. O. (1994), Structure and petroleum potential of the Dagestan thrust belt, northeastern Caucasus, Russia, *Bulletin of Canadian Petroleum Geology*, *42*(3), 352-364.

Sobornov, K. O. (1996), Lateral variations in structural styles of tectonic wedging in the northeasteren Caucasus, *Bulletin of Canadian Petroleum Geology*, *44*(2), 385-399.

Somin, M. L. (2011), Pre-Jurassic basement of the Greater Caucasus: Brief overview, *Turkish Journal of Earth Sciences*, *20*, 545-610.

Somin, M. L., E. N. Lepekhina, and A. N. Konilov (2007), Age of th high-temperature gneiss core of the central Caucasus, *Dokl. Earth Sc.*, *415*(5), 690-694.

Somin, M. L., A. B. Kotov, E. B. Sal'nikova, O. A. Levchenkov, A. N. Pis'mennyi, and S. Z. Yakovleva (2006), Paleozoic rocks in infrastructure of the metamorphic core,

the Greater Caucasus Main Range Zone, *Stratigraphy and Geological Correlation*, *14*(5), 475-485.
Sosson, M., et al. (2010), Subductions, obduction and collision in the Lesser Caucasus (Armenia, Azerbaijan, Georgia), new insights, *Geological Society, London, Special Publications*, *340*(1), 329-352.
Stampfli, G. M., and G. D. Borel (2002), A plate tectonic model for the Paleozoic and Mesozoic constrained by dynamic plate boundaries and restored synthetic oceanic isochrons, *Earth and Planetary Science Letters*, *196*(1–2), 17-33.
Talebian, M., and J. Jackson (2002), Offset on the Main Recent Fault of NW Iran and implications for the late Cenozoic tectonics of the Arabia-Eurasia collision zone, *Geophysical Journal International*, *150*, 422-439.
Talling, P. J., L. A. Amy, R. B. Wynn, G. Blackbourn, and O. Gibson (2007), Evolution of Turbidity Currents Deduced from Extensive Thin Turbidites: Marnoso Arenacea Formation (Miocene), Italian Apennines, *J Sediment Res*, *77*(3), 172-196.
Taylor, B., and G. D. Karner (1983), On the evolution of marginal basins, *Reviews of Geophysics*, *21*(8), 1727-1741.
Trexler, C. C., E. Cowgill, N. A. Niemi, and T. Godoladze (2015), Exploring subduction, slab breakoff, and upper-plate deformation in the Georgian Greater Caucasus: Shortening estimates from area- and line-balanced crustal scale cross sections, paper presented at American Geophysical Union Fall Meeting Abstract T31B-2886, American Geophysical Union, San Francisco.
van Hinsbergen, D. J. J., P. Kapp, G. Dupont-Nivet, P. C. Lippert, P. G. DeCelles, and T. H. Torsvik (2011), Restoration of Cenozoic deformation in Asia and the size of Greater India, *Tectonics*, *30*(5), TC5003.
van Hinsbergen, D. J. J., P. C. Lippert, G. Dupont-Nivet, N. McQuarrie, P. V. Doubrovine, W. Spakman, and T. H. Torsvik (2012), Greater India Basin hypothesis and a two-stage Cenozoic collision between India and Asia, *Proceedings of the National Academy of Sciences*, *109*(20), 7659-7664.
Vermeesch, P. (2012), On the visualisation of detrital age distributions, *Chemical Geology*, *312–313*, 190-194.
Vezzoli, G., E. Garzanti, S. J. Vincent, S. Andò, A. Carter, and A. Resentini (2014), Tracking sediment provenance and erosional evolution of the western Greater Caucasus, *Earth Surface Processes and Landforms*, *39*(8), 1101-1114.
Vincent, S. J., F. Hyden, and W. Braham (2014), Along-strike variations in the composition of sandstones derived from the uplifting western Greater Caucasus: causes and implications for reservoir quality prediction in the Eastern Black Sea, *Geological Society, London, Special Publications*, *386*(1), 111-127.
Vincent, S. J., A. C. Morton, F. Hyden, and M. Fanning (2013), Insights from petrography, mineralogy and U–Pb zircon geochronology into the provenance and

reservoir potential of Cenozoic siliciclastic depositional systems supplying the northern margin of the Eastern Black Sea, *Marine and Petroleum Geology*, *45*(0), 331-348.

Vincent, S. J., A. C. Morton, A. Carter, S. Gibbs, and T. G. Barabadze (2007), Oligocene uplift of the Western Greater Caucasus: an effect of initial Arabia-Eurasia collision, *Terra Nova*, *19*, 160-166.

Vincent, S. J., M. B. Allen, A. Ismail-Zadeh, R. Flecker, K. A. Foland, and M. Simmons (2005), Insights from the Talysh of Azerbaijan into the Paleogene evolution of the South Caspian region, *Geological Society of America Bulletin*, *117*(11/12), 1513-1533.

Vincent, S. J., A. Carter, V. A. Lavrishchev, S. P. Rice, T. G. Barabadze, and N. Hovius (2011), The exhumation of the western Greater Caucasus: a thermochronometric study, *Geological Magazine*, *148*(01), 1-21.

Wang, C. Y., I. H. Campbell, A. S. Stepanov, C. M. Allen, and I. N. Burtsev (2011), Growth rate of the preserved continental crust: II. Constraints from Hf and O isotopes in detrital zircons from Greater Russian Rivers, *Geochimica et Cosmochimica Acta*, *75*(5), 1308-1345.

Weislogel, A. L. (2008), Tectonostratigraphic and geochronologic constraints on evolution of the northeast Paleotethys from the Songpan-Ganzi complex, central China, *Tectonophysics*, *451*(1–4), 331-345.

Weislogel, A. L., S. A. Graham, E. Z. Chang, J. L. Wooden, G. E. Gehrels, and H. Yang (2006), Detrital zircon provenance of the Late Triassic Songpan-Ganzi complex: Sedimentary record of collision of the North and South China blocks, *Geology*, *34*(2), 97-100.

Westaway, R. (1994), Present-day kinematics of the Middle East and eastern Mediterranean, *Journal of Geophysical Research*, *99*(B6), 12071-12090.

Willett, S., C. Beaumont, and P. Fullsack (1993), Mechanical model for the tectonics of doubly vergent compressional orogens, *Geology*, *21*(4), 371-374.

Wynn, R. B., P. P. E. Weaver, D. G. Masson, and D. A. V. Stow (2002), Turbidite depositional architecture across three interconnected deep-water basins on the north-west African margin, *Sedimentology*, *49*(4), 669-695.

Yakovlev, P. V., and M. K. Clark (2014), Conservation and redistribution of crust during the Indo-Asian collision, *Tectonics*, *33*(6), 2013TC003469.

Yilmaz, A., S. Adamia, A. Chabukiani, T. Chkhotua, K. Erdogan, S. Tuzcu, and M. Karabiyikoglu (2000), Structural correlation of the southern Transcaucasus (Georgia)-eastern Pontides (Turkey), in *Tectonics and Magmatism in Turkey and the Surrounding Area*, edited by E. Bozkurt, J. A. Winchester and J. D. A. Piper, pp. 171-182, Geological Society of London Special Pubications 173, London.

Yilmaz, Y. (1993), New evidence and model on the evolution of the southeast Anatolian orogen, *Geological Society of America Bulletin*, *105*(2), 251-271.

Zakariadze, G. S., Y. Dilek, S. A. Adamia, R. E. Oberhänsli, S. F. Karpenko, B. A. Bazylev, and N. Solov'eva (2007), Geochemistry and geochronology of the Neoproterozoic Pan-African Transcaucasian Massif (Republic of Georgia) and implications for island arc evolution of the late Precambrian Arabian–Nubian Shield, *Gondwana Research*, *11*(1–2), 92-108.

Zdilashavili, V. Y. (1957), K-37-XII, Ministry of Geology and Mineral Protection USSR, Moscow.

Zonenshain, L. P., and X. Le Pichon (1986), Deep basins of the Black Sea and Caspian Sea as remnants of Mesozoic back-arc basins, *Tectonophysics*, *123*, 181-211.

Zonenshain, L. P., M. I. Kuzmin, L. M. Natapov, and B. M. Page (1990), Alpine-Himalayan Foldbelt Within the USSR, in *Geology of the USSR: A Plate-Tectonic Synthesis*, edited, pp. 168-198, American Geophysical Union.

Zor, E. (2008), Tomographic evidence of slab detachment beneath eastern Turkey and the Caucasus, *Geophysical Journal International*, *175*(3), 1273-1282.

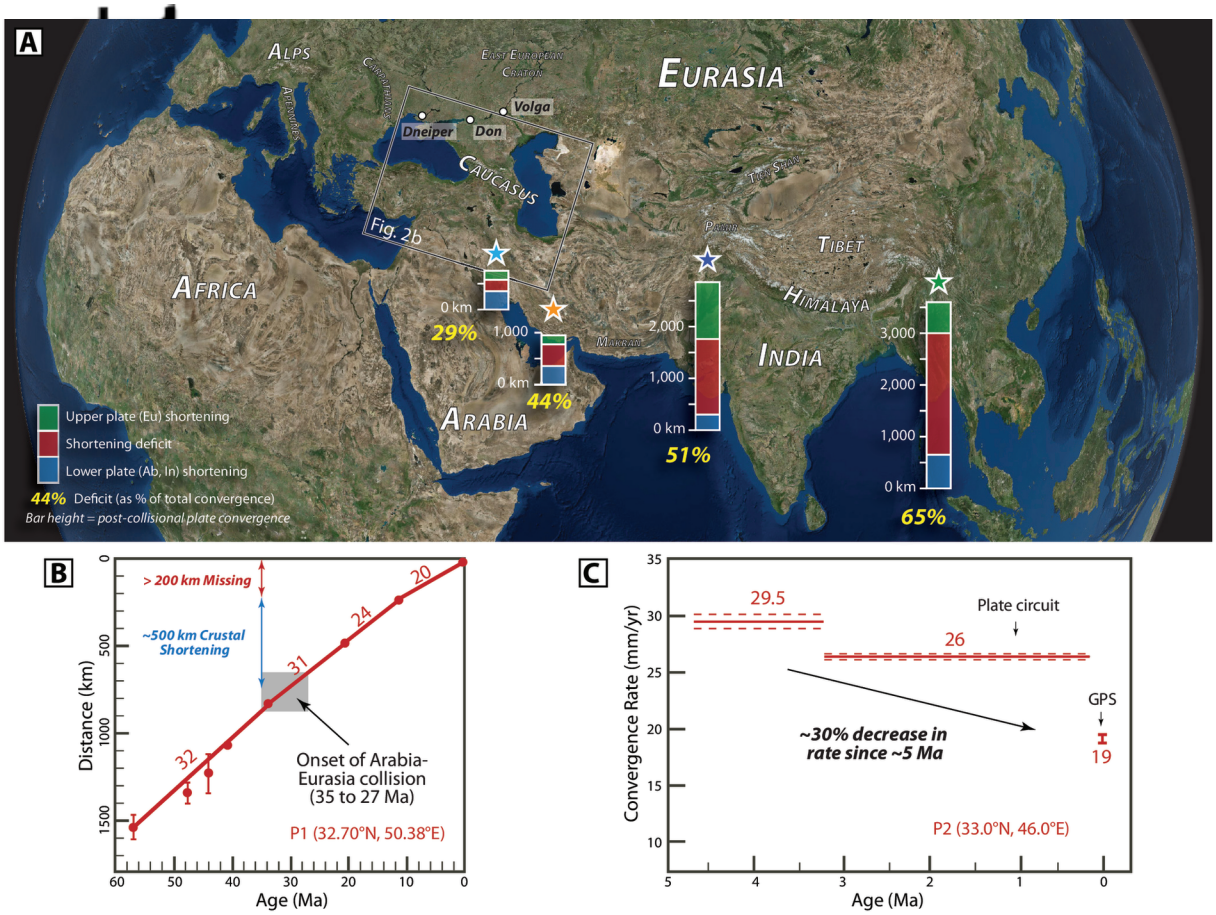

Figure 1. (a) Comparison of crustal - shortening deficits in the Arabia - Eurasia and India - Eurasia collisions within the Alpine-Himalaya belt [modified from van Hinsbergen et al., 2012]. Total bar height indicates amount of post-collisional plate convergence expected at the lower-plate reference points (locations approximated by stars). Green and blue bars show amount of observed upper- and lower-plate crustal shortening, respectively. Red bars indicate apparent shortening deficits. Values for India - Eurasian collision are from van Hinsbergen et al. [2012]; convergence and shortening-deficit information for Arabia - Eurasia collision are from Hatzfeld and Molnar [2010] and McQuarrie and van Hinsbergen [2013]. White dots indicate detrital zircon samples of modern rivers draining East European Craton reported by Wang et al. [2011]. Base image is the World Imagery Basemap Layer from ESRI. (b) Plot showing distance Arabian reference point P1 (Figure 2b) traveled relative to Eurasia over time [after Hatzfeld and Molnar, 2010]. Numbers above line segments give incremental convergence rates (in mm/y). Gray box spans range of current estimates for age of onset of Ab-Eu collision; lower-left and upper-right corners indicate the maximum (~900 km) and minimum (~700 km) magnitudes of post-collisional Ab-Eu convergence, respectively. Arrows indicate the > 200 km difference (red arrow) between magnitude of post-collisional convergence (700 to 900 km, gray box) and estimated upper-plate shortening (~500 km, blue arrow) reported by McQuarrie and van Hinsbergen [, 2013]. (c) Plot of Ab-Eu convergence rate over time for reference point P2 (Figure 2b) [after Austermann and Iaffaldano, 2013]. Red lines with dashed confidence bounds are computed from a plate circuit, the point with error bars is determined from GPS geodesy. Note the ~30% decrease in Ab-Eu convergence rate over the last 5 Ma. Rates at ~5Ma differ between the two panels (i.e., 20 mm/yr in B and 30 mm/yr in C) because they were computed using different stages (and thus average over different time intervals), reference points, and rotation poles [e.g., see details in Austermann and Iaffaldano, 2013; McQuarrie et al., 2003].

2016tc004295-f01-z-.eps

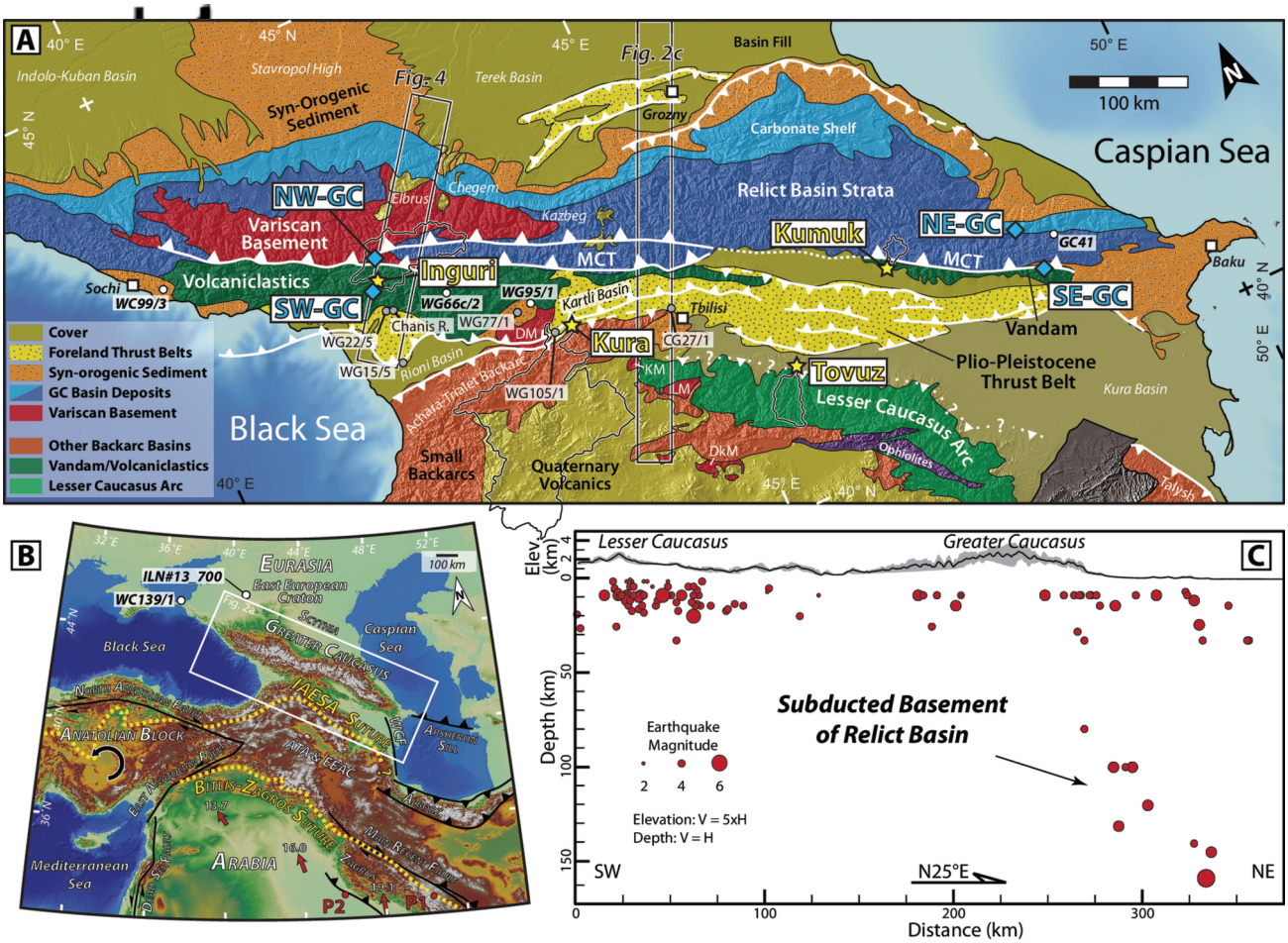

Figure 2. (a) Simplified tectonic map of Greater and Lesser Caucasus, showing locations of main structures and new U-Pb detrital zircon samples (diamonds: bedrock sandstone; stars: modern river sediment, with catchments delineated by black lines edged in white). Dots denote locations of previously reported detrital zircon [white fill, Allen et al., 2006; Vincent et al., 2013] and provenance analyses [gray fill, Vincent et al., 2014; Vincent et al., 2013; Vincent et al., 2007] discussed in text; see Figure 6 for additional sample numbers. Fault geometries are simplified on northern margin of central Greater Caucasus and shown as north-directed thrusts; true geometries are south-directed backthrusts above a triangle zone at the leading edge of a generally north-directed thrust system [e.g., Sobornov, 1994; Sobornov, 1996]. MCT: Main Caucasus Thrust. Basement massifs: DM – Dzirula, KM – Khrami, LM – Loki, and DkM – Dzarkuniatz. Boxes indicate locations of cross sections in Figures 2c and 4. (b) Map of Arabia-Eurasia collision zone; black lines indicate major structural systems; red arrows show motion of Arabia relative to Eurasia from the 2010 GEODVEL model, with numbers indicating rates in mm/yr [Argus et al., 2010]; red dots are reference points for plots of plate convergence (P1) and rate (P2) over time (see Figure 1); white dots are published detrital zircon samples from Oligo-Pliocene sandstone [Vincent et al., 2013]; dashed yellow lines indicate Bitlis and Izmir-Ankara-Erzincan-Sevan-Akera (IAESA) sutures [Rolland et al., 2012] bounding the ATA (Anatolide-Tauride-Armenian) block, which contains the South Armenian Block and is bound to the south by the East Anatolian Accretionary Complex (EAAC). WCF: West Caspian Fault [Allen et al., 2003]. (c) North-dipping zone of earthquakes extending to ~160 km beneath the Greater Caucasus indicates subducted basement of the relict ocean basin. Panels a-b after Forte et al. [2014]; Panel c after Mumladze et al. [2015].

2016tc004295-f02-z-.eps

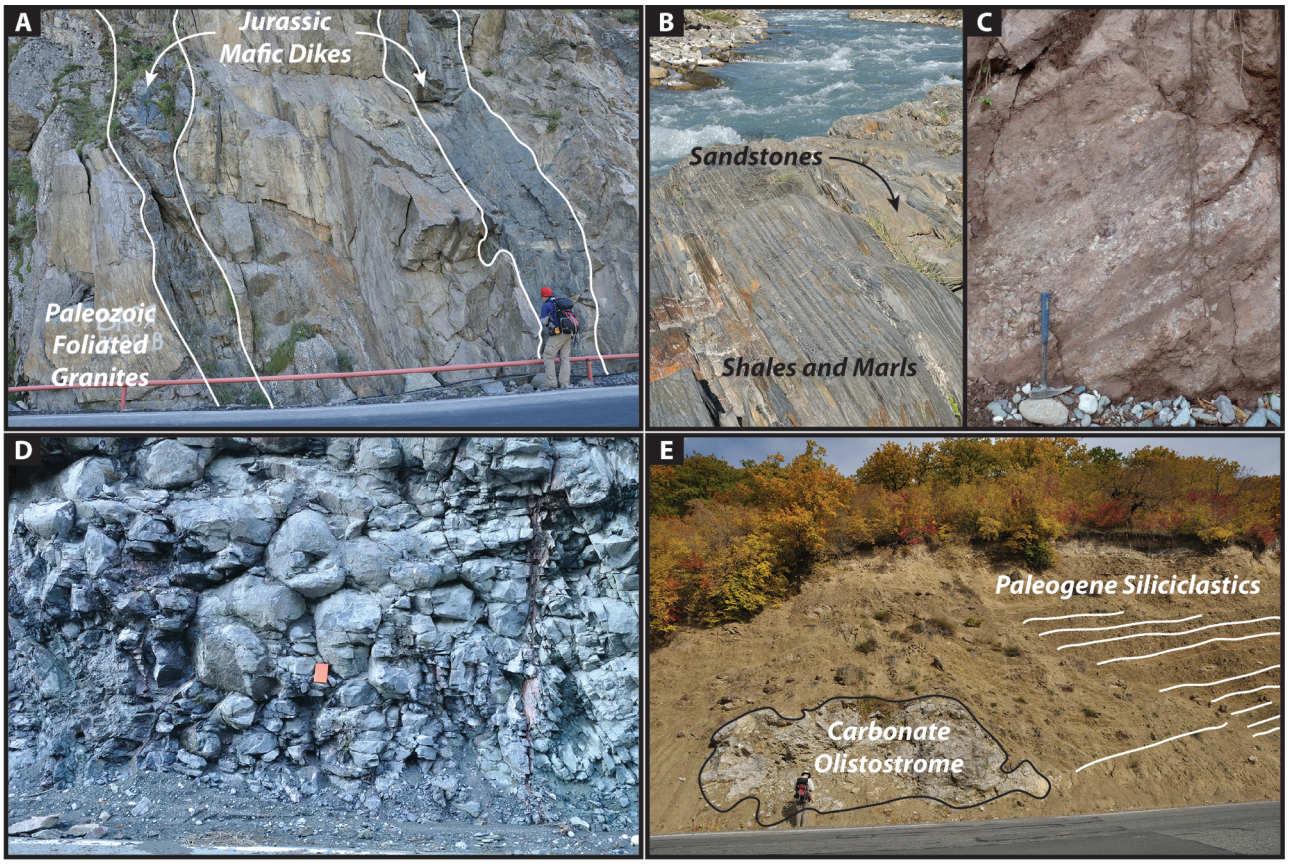

Figure 3. Field photographs showing units and structural relations at locations indicated in Figure S1. (a) Foliated Variscan basement gneiss intruded by foliation-parallel mafic dikes of inferred Middle Jurassic age in the hanging wall of the Main Caucasus Thrust. Unit ages from Gubkina and Ermakov [1989]. (b) Flyschoid sedimentary rocks south of the Main Caucasus Thrust reported to be either Early-Middle Jurassic [Kandelaki and Kakhazdze, 1957] or Early Cretaceous (Hauterivian) [Gudjabidze, 2003] in age. (c) Volcaniclastic conglomerate and breccia of Late Jurassic (Kimmeridgian) age [Melnikov and Popova, 1975] in the southwestern part of the Greater Caucasus thrust belt. (d) Pillow basalts of Early to Middle Jurassic age [Melnikov and Popova, 1975] within the thrust belt. (e) Well-bedded, coarse-grained siliciclastic deposits of Late Cretaceous to Eocene age [Kandelaki and Kakhazdze, 1957] hosting olistostromes containing blocks of probable Cretaceous-aged carbonate.

2016tc004295-f03-z-.eps

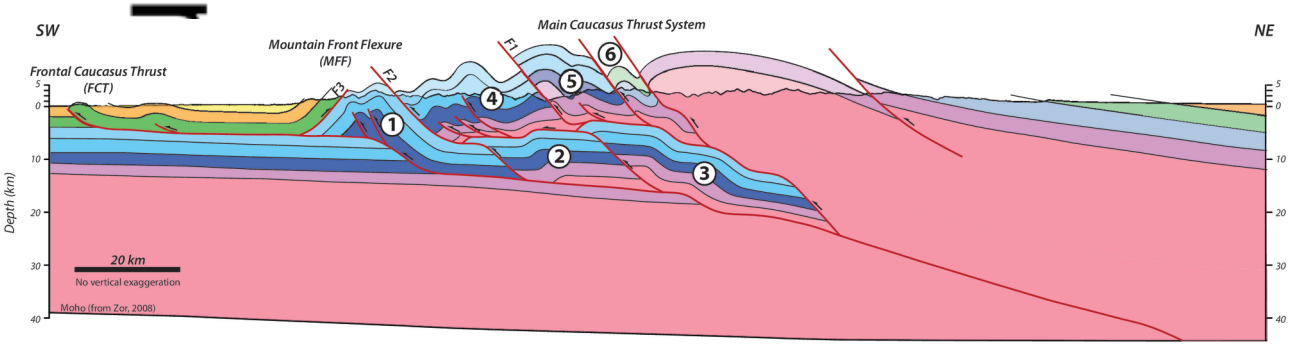

Figure 4. Preliminary line-length balanced regional cross section across the western Greater Caucasus at ~42°E at location shown in Figure 2a. Section was constructed from the surface geology as reported on 1:200,000-scale Soviet geologic map sheets K38-XIII [Dzhanelidze and Kandelaki, 1957], K38-VIII [Melnikov and Popova, 1975], K38-VII [Gamkrelidze and Kakhazdze, 1959], K38-II [Kizevalter, 1959], K38-I [Potapenko, 1964], K37-XVIII [Kandelaki, 1957], and K37-XII [Zdilashavili, 1957]. Moho depth from Zor [2008]. Total shortening of ~130 km is determined by line-length balancing the basement-cover contact between the pink and purple units. The retro-deformable nature of this cross section makes it a step forward in quantifying shortening estimates in the Greater Caucasus over previous sections [e.g., Dotduyev, 1986]. However, ongoing geologic mapping in the vicinity of the surface trace of this cross section indicates that future refinement of this shortening estimate is expected [e.g., Trexler et al., 2015].

2016tc004295-f04-z-.eps

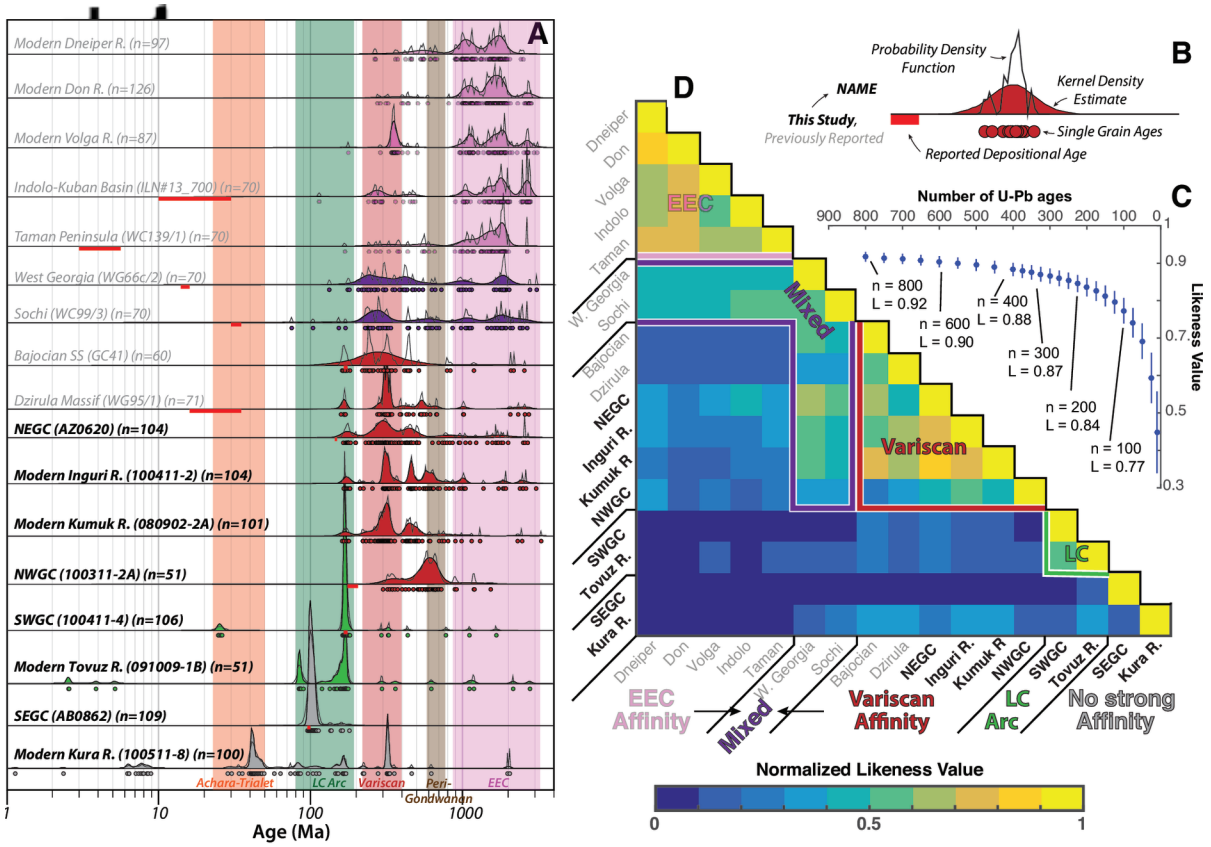

Figure 5. Detrital zircon U-Pb ages from the Caucasus region and an analysis of their provenance implications. Bold sample names indicate results from the present study, those in gray are published analyses of 5 Oligo-Pliocene sandstones [Vincent et al., 2013], modern sediment from the Dnieper, Don, and Volga rivers [Wang et al., 2011], and 1 Jurassic (Bajocian) sandstone [Allen et al., 2006]. See Figures 1a and 2a for sample locations. Note separation of samples into distinct northern (Variscan and East European Craton) and southern (Lesser Caucasus and Achara-Trialet) provenance domains. All southern samples show minimal evidence of contribution from the northern source (i.e., SE-GC, SW-GC and Tovuz River), except for Miocene sandstone samples (WG95/1 and WG66c/2), which are inferred here to have been deposited out in the Greater Caucasus Basin after it started to close. Modern sediments from rivers draining the Greater Caucasus (Inguri, Kumuk, Kura) reflect mixing of northern and southern sources, indicating their catchments span both domains. Modern sediments from Russian rivers draining the East European Craton show provenance patterns that are largely distinct from the Caucasus samples, as noted previously [Allen et al., 2006; Vincent et al., 2013]. (a) Age spectra shown as PDP and KDE curves [Vermeesch, 2012]; see panel b for legend. Samples are grouped and colored according to source areas determined in panel D from analysis of likeness (L) values [Satkoski et al., 2013]. Red boxes indicate reported depositional ages, vertical colored bars indicate age spans inferred to be diagnostic of particular source areas, with blue and green bars denoting the northern (Variscan) and southern (Lesser Caucasus) source areas, respectively. (b) Legend explaining symbols used on panel a. (c) Plot showing maximum possible likeness value (L) as a function of sample size n (number of U-Pb ages in the detrital zircon sample), determined by sampling with replacement from a 4000-grain detrital zircon age dataset [Pullen et al., 2014]. Note that L increases with increasing n, but rate of increase decreases with n > 300. (d) Correlation matrix of normalized likeness values (L) for all samples. Four groups of samples can be defined on the basis of the L-value correlation: East European Craton, Variscan, Mixed (East European Craton + Variscan), and Lesser Caucasus (see text for discussion).

2016tc004295-f05-z-.eps

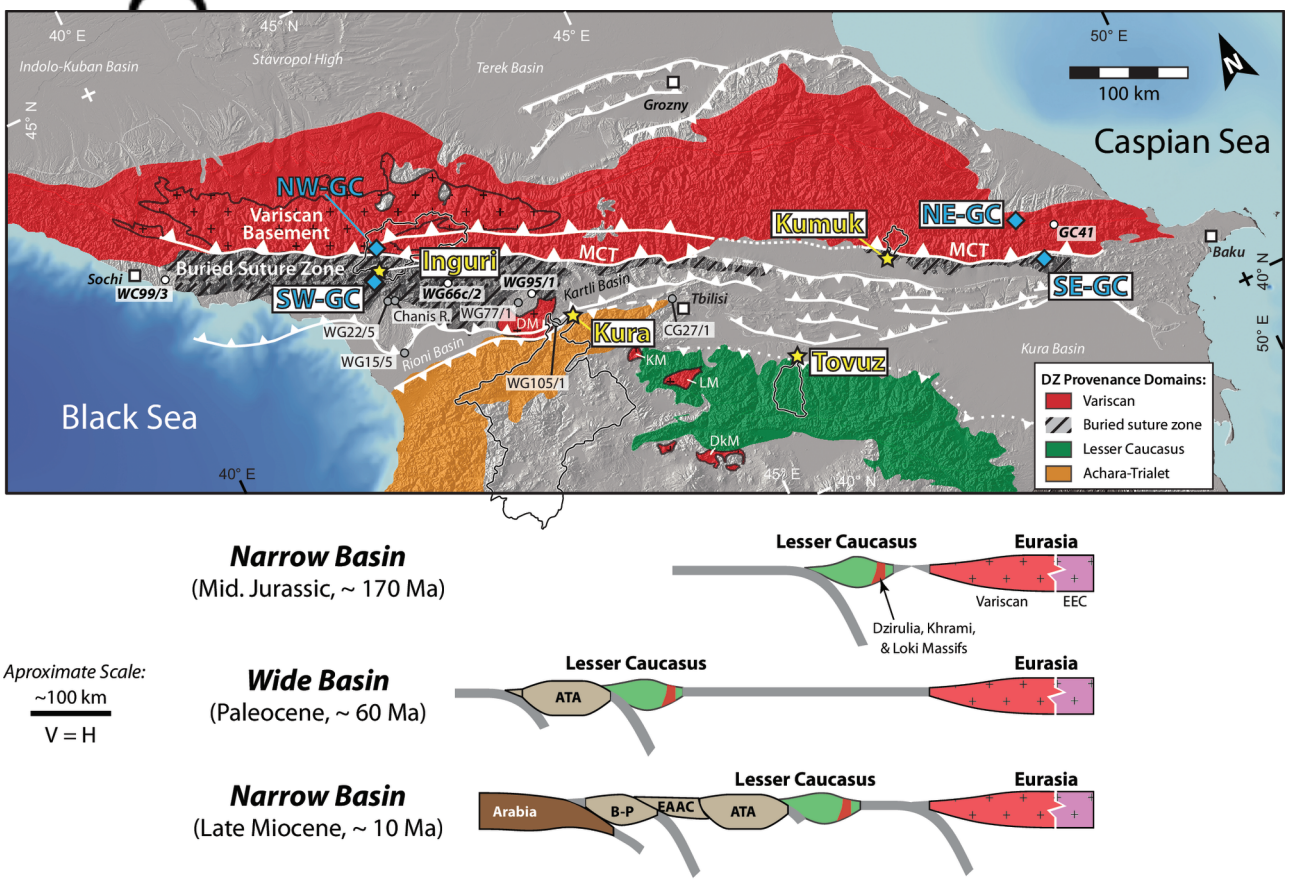

Figure 6. Sample locations with respect to detrital zircon provenance domains and inferred buried suture zone (geometry approximate). The location of the suture is too poorly known to show it as a discrete line, although current data indicate it is buried somewhere within the indicated zone. Additional field investigation is required to refine the location and surficial expression of the buried suture, and determine how the basin geometry evolved over time. Colors for Variscan, Lesser Caucasus, and Achara-Trialet provenance domains correspond to those used in Figure 2a. Regions concealed by younger synorogenic and Plio-Quaternary sediments shown in light gray. Diamonds and stars indicate detrital zircon samples of bedrock sandstone and modern river sediment, respectively; black lines with white edges delineate catchments above modern river samples. White dots indicate previously reported detrital zircon analyses of Oligo-Miocene [Vincent et al., 2013] and Jurassic (Bajocian) [Allen et al., 2006] sandstone. Gray dots show locations of other published provenance data discussed in text, including 3 samples at the Chanis River section (WG28b/3, WG28c/5, WG28c/1, and WG27/4) [Vincent et al., 2014; Vincent et al., 2013; Vincent et al., 2007]. Schematic cross sections indicate that basin was wide during latest Cretaceous to Paleocene time, but narrow both during Jurassic opening and late Miocene closure (ATA: Anatolide-Tauride-Armenian block; B-P: Bitlis-Pötürge; EAAC: East Anatolian Accretionary Complex).

2016tc004295-f06-z-.eps

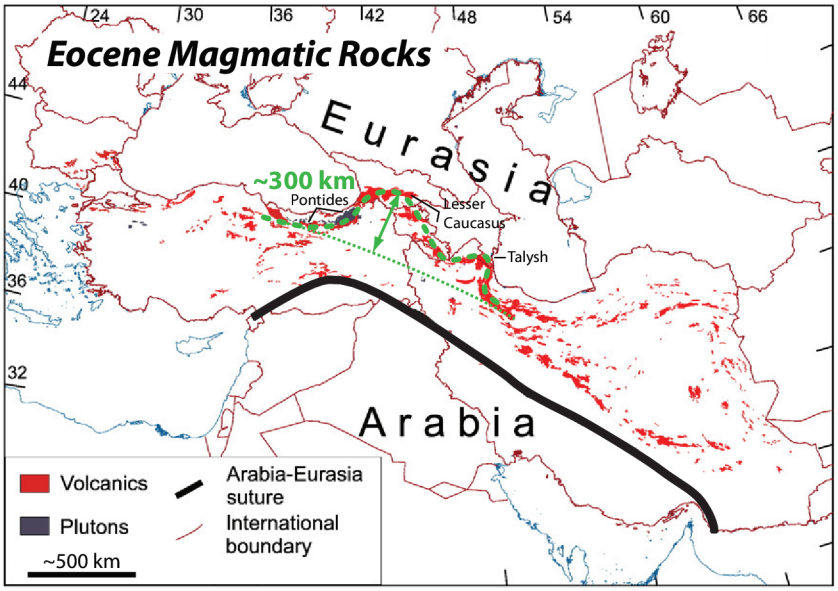

Figure 7. Map of Eocene magmatic rocks in Asia Minor showing a salient in the Lesser Caucasus and Talysh relative to the Pontides and Alborz to the west and east, respectively. Thick green dotted line indicates a rough estimate of the current (deformed) geometry, which appears to be deflected to the northeast by as much as 300 km relative to an assumed original geometry (thin green dotted line), prior to closure of the Greater Caucasus Basin [modified from Allen and Armstrong, 2008]. Heavy black line shows position of Bitlis-Zagros suture at present only. During Eocene this suture was well south of the position shown here at a location not restored in the figure. Because only Eocene rocks are shown, any bending that occurred to produce the pattern shown here must postdate any earlier phases of oroclinal bending implied by paleomagnetic data [e.g., Meijers et al., 2016 in press]. The significance of the apparent eastward decrease in deflection magnitude in the Talysh is unclear. The original geometry of the belt is not well known and it may be that the thin green dotted line should be farther south at ~48°E. Alternatively, the Greater Caucasus basin may have narrowed eastwards. The reconstruction here is not precluded by Eocene magmatic rocks south of the dotted line that are due to other Neotethyan arcs/basins south of the Lesser Caucasus-Talysh system.

2016tc004295-f07-z-.eps

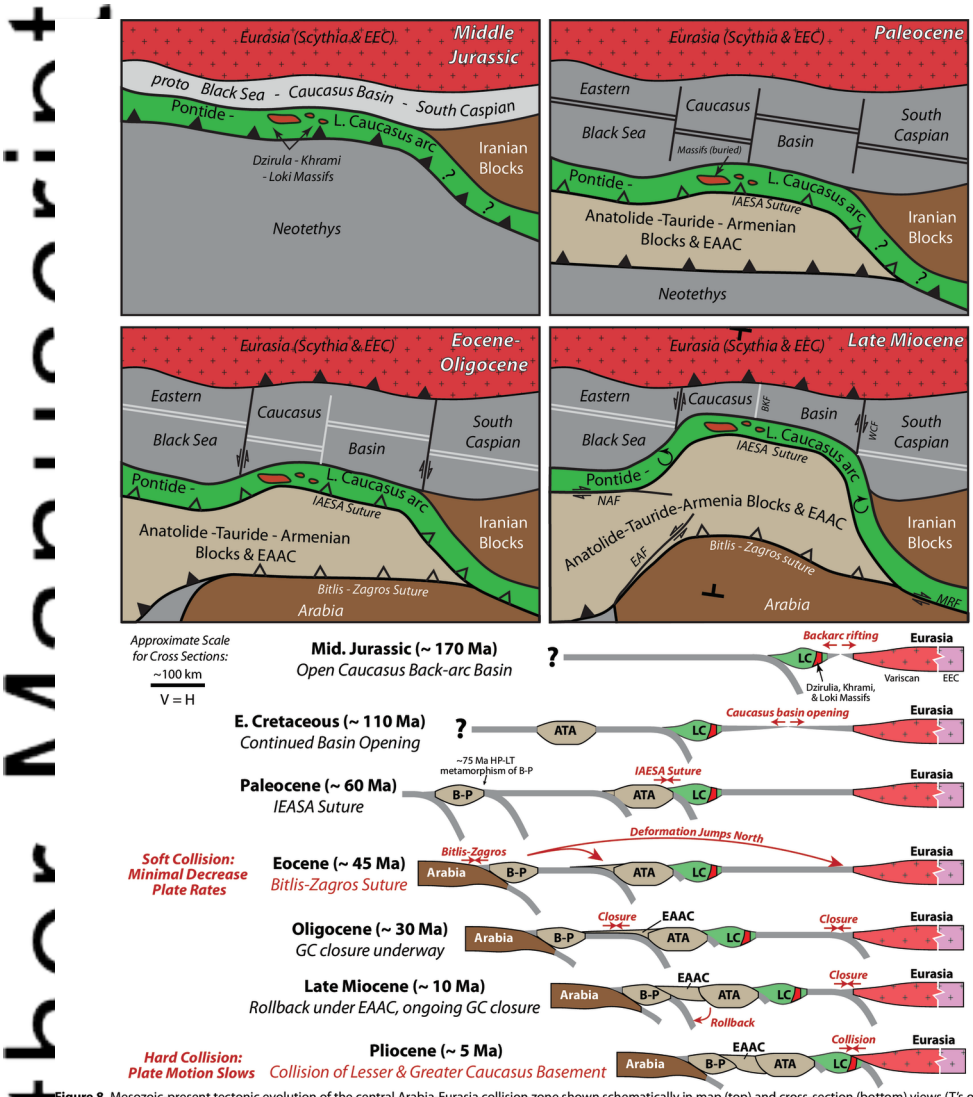

Figure 8. Mesozoic-present tectonic evolution of the central Arabia-Eurasia collision zone shown schematically in map (top) and cross-section (bottom) views (T's on late Miocene map indicate approximate location of section). Middle Jurassic: backarc rifting of the Pontide-Lesser Caucasus arc opens the Black Sea, Caucasus, and South Caspian basins. Light gray color represents extended continental crust and/or transitional oceanic crust. Paleocene: The IAESA (Sevan) suture had either already closed in the latest Cretaceous (~73-71 Ma) [Rolland et al., 2009; Rolland et al., 2012] or did so in Paleocene time [Sosson et al., 2010] via collision of the Lesser Caucasus arc and Anatolide-Tauride-Armenian. Eocene-Oligocene: closure of the Bitlis suture results in soft collision between Arabia and the Bitlis-Pötürge massif, causing the locus of convergence to jump northward, initiating subduction of the Caucasus relict back-arc basin. Oligo-Miocene: Ab-Eu plate convergence accommodated by subduction of the Greater Caucasus Basin beneath the Greater Caucasus and growth of East Anatolian Accretionary Complex, with minimal reduction in plate convergence rate. Mio-Pliocene: collision of the Lesser Caucasus arc with the Eurasian basement to the north at ~5 Ma leads to hard collision and accelerated uplift/exhumation of the Greater Caucasus Mountains. Geometries of ridges (paired lines) and transforms (single lines) in backarc basin are completely conjectural (black = active rifting, grey = relict). Black Sea geometry simplified by omission of Shatsky Ridge. Arrowed semi-circles indicate inferred vertical-axis rotation and oroclinal bending of Pontide-Lesser Caucasus Arc. Barbed lines indicate subduction (solid) or sutures (hollow), barbs on upper plate. ATA: Anatolide-Tauride-Armenian block; B-P: Bitlis-Pötürge; BKF: Borjomi-Kazbegi fault; EAAC: East Anatolian Accretionary Complex; EAF: East Anatolian fault; GC: Greater Caucasus; LC: Lesser Caucasus; MRF: Main Recent Fault; NAF: North Anatolian fault; WCF: West Caspian fault. Adapted from Zonenshain and Le Pichon [1986], Şengör et al. [2003], Sosson et al. [2010], Rolland et al. [2012], Allen et al. [2003], Allen and Armstrong [2008], and Stampfli and Borel [2002].

2016tc004295-f08-z-.eps

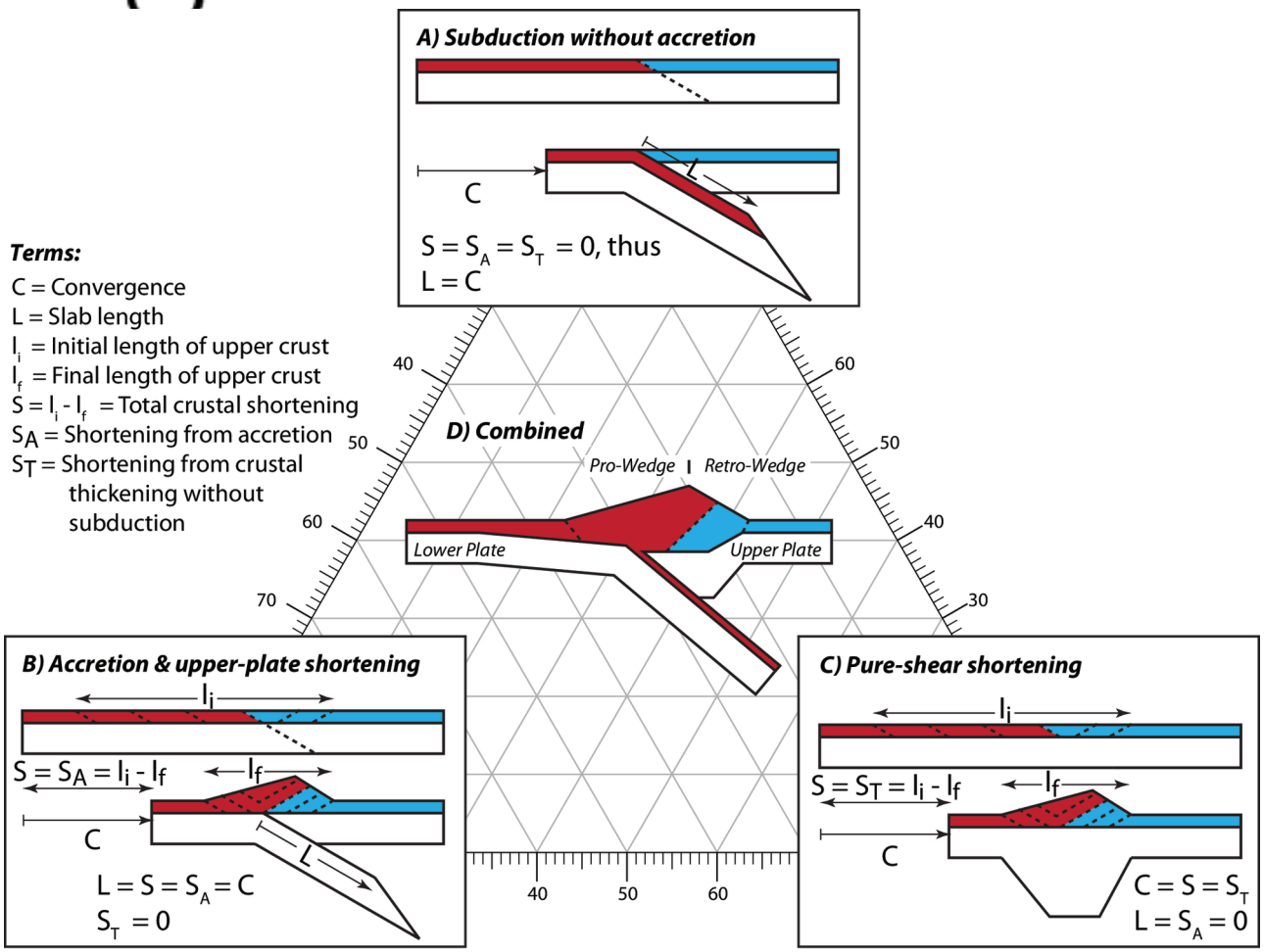

Figure 9. Both deficits and balances of upper crustal shortening should be expected within collisional orogens. Diagrams show the distribution of plate convergence into end-member components of (a) subduction without accretion, which produces no crustal shortening, (b) subduction with full accretion, in which convergence is fully recorded by crustal shortening, and (c) pure shear shortening of the orogen, which shortens the crust but does not contribute to subduction. The center panel (d) shows the most general case, where all three mechanisms operate simultaneously. In this general case, it is possible for plate convergence to either be equal to or exceed crustal shortening. Likewise, crustal shortening can be less than, equal to, or greater than the length of slab subducted since collision.

2016tc004295-f09-z-.eps